JCI The Journal of Clinical Investigation

TPL2 enforces *RAS*-induced inflammatory signaling and is activated by point mutations

Paarth B. Dodhiawala, Namrata Khurana, Daoxiang Zhang, Yi Cheng, Lin Li, Qing Wei, Kuljeet Seehra, Hongmei Jiang, Patrick M. Grierson, Andrea Wang-Gillam, Kian-Huat Lim

J Clin Invest. 2020. https://doi.org/10.1172/JCI137660.

Research In-Press Preview **Inflammation** **Oncology**

Graphical abstract

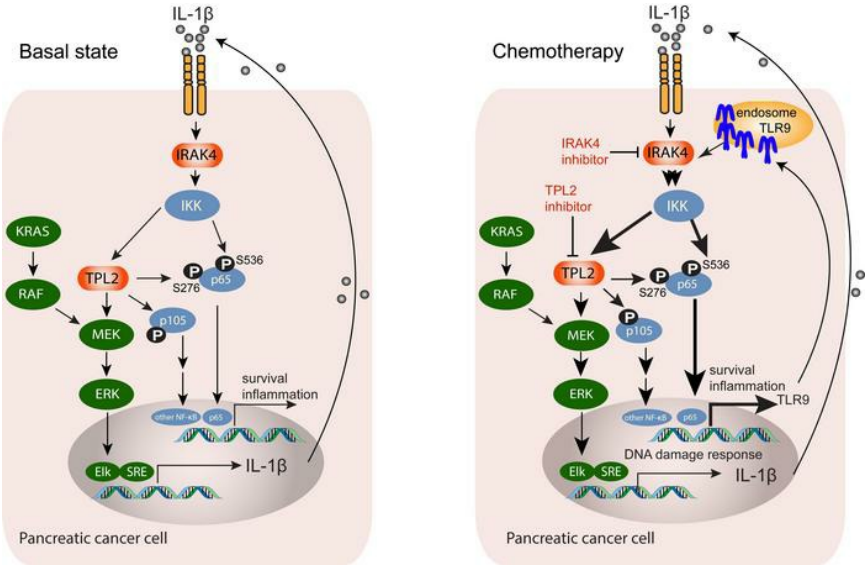

Find the latest version:

https://jci.me/137660/pdf

TPL2 enforces *RAS*-induced inflammatory signaling and is activated by point mutations

Paarth B. Dodhiawala[1], Namrata Khurana[1], Daoxiang Zhang[1], Yi Cheng[1], Lin Li[1], Qing Wei[1,2], Kuljeet Seehra[1], Hongmei Jiang[1], Patrick M. Grierson[1], Andrea Wang-Gillam[1], Kian-Huat Lim[1,*]

[1]Division of Oncology, Department of Internal Medicine, Barnes-Jewish Hospital and The Alvin J. Siteman Comprehensive Cancer Center, Washington University School of Medicine, St. Louis, MO 63110, USA.

[2]Department of Laboratory Medicine, Renji Hospital, School of Medicine, Shanghai Jiaotong University, Shanghai, 200127, China.

The authors have declared that no conflict of interest exists

*Corresponding author:

Kian-Huat Lim

Washington University School of Medicine

660 South Euclid Avenue

Campus Box 8069

Saint Louis, MO 63110

Tel: 314-362-6157

Fax: 314-747-9329

Email: kian-huat.lim@wustl.edu

ABSTRACT

NF-κB transcription factors, driven by the IRAK-IKK cascade, confer treatment resistance in pancreatic ductal adenocarcinoma (PDAC), a cancer characterized by near universal *KRAS* mutation. Through reverse-phase protein array and RNAseq we discovered IRAK4 also contributes substantially to MAPK activation in *KRAS*-mutant PDAC. IRAK4 ablation completely blocked *RAS*-induced transformation of human and murine cells. Mechanistically, expression of mutant *KRAS* stimulated an inflammatory, autocrine IL-1β signaling loop that activated IRAK4 and MAPK pathway. Downstream of IRAK4, we uncovered TPL2/MAP3K8 as the essential kinase that propels both MAPK and NF-κB cascades. Inhibition of TPL2 blocked both MAPK and NF-κB signaling, and suppressed *KRAS*-mutant cell growth. To counter chemotherapy-induced genotoxic stress, PDAC cells upregulated TLR9, which activated pro-survival IRAK4-TPL2 signaling. Accordingly, TPL2 inhibitor synergized with chemotherapy to curb PDAC growth in vivo. Finally, from TCGA we characterized two *MAP3K8* point mutations that hyperactivate MAPK and NF-κB cascades by impeding TPL2 protein degradation. Cancer cell lines naturally harboring these *MAP3K8* mutations are strikingly sensitive to TPL2 inhibition, underscoring the need to identify these potentially targetable mutations in patients. Overall, our study establishes TPL2 as a promising therapeutic target in *RAS*- and *MAP3K8*-mutant cancers and strongly prompts development of TPL2 inhibitors for pre-clinical and clinical studies.

INTRODUCTION

Targeting the RAS oncoproteins remains unfulfilled in the clinic. While the newly developed $KRAS^{G12C}$ inhibitor has achieved considerable success in lung cancer(1), it is ineffective in other *$KRAS^{G12C}$*-mutant cancer types such as colon cancer. In addition, HRAS, NRAS and non-G12C KRAS oncoproteins remain undruggable. In pancreatic ductal adenocarcinoma (PDAC), though KRAS mutations are virtually universal, the *G12C* mutation is rare(2). Strategies to target KRAS effectors including the mitogen-activated protein kinase (MAPK) and phosphoinositide 3-kinase (PI3K) cascades are unsuccessful(3) and multiple resistance mechanisms have been described explaining their failures. Aberrant activation of the NF-κB transcription factors, especially the RELA (or p65) family member, occurs in approximately two-thirds of PDAC and is a major mechanism that underlies the aggressive nature of PDAC(4-7). In a genetically-engineered mouse model (GEMM), ablation of IKKβ kinase, which activates the NF-κB members, completely abolished *$KRAS^{G12D}$*-induced PDAC development(8). However, development of IKK inhibitors is hampered by clinical toxicities and off-target effects(9). PDAC cells and the surrounding stromal fibroblasts secrete IL-1β that engages interleukin-1 receptor-associated kinase 4 (IRAK4) to drive IKKβ and the NF-κB pathway(10), indicating IRAK4 is a promising therapeutic target. IRAK4 is a critical signal transducer downstream of the innate immune receptors including the Toll-like(TLR) and IL-1 (IL-1R) receptors(11). When engaged, these receptors recruit MYD88 and IRAK1 as adaptors, forming a platform that recruits IRAK4. IRAK4 then activates the IKK complex, allowing cytoplasmic NF-κB subunits such as RELA/p65 and p50 to enter the nucleus and transactivate inflammatory and survival genes(12). The pro-tumorigenic role of this pathway has been described in melanoma(13), breast(14), head and neck (15), colon(16) and pancreatic cancers(7, 10). However, these studies do not describe the genetic context in which IRAK4 inhibition is most likely to succeed, nor do they provide insights into the crosstalk of IRAK4 signaling with other oncogenic events besides the NF-κB pathway.

In this study, we interrogated The Cancer Genome Atlas (TCGA) database and identified *MYD88, IRAK1* and *IRAK4* are associated with *RELA* expression and poor prognosis in PDAC. We further found

IRAK4 is essential for *RAS*-induced oncogenic transformation. Interestingly, by unbiased reverse-phase protein array and RNAseq we discovered signaling crosstalk between IRAK4 and the MAPK pathway in *KRAS*-mutant PDAC cells. We elucidate the mechanism of how oncogenic KRAS activates IRAK4, and uncover Tumor Progression Locus 2 (TPL2, also known as MAP3K8 or COT) as the essential kinase that controls both MAPK and NF-κB cascades downstream of IRAK4 and effectively KRAS. In addition, we interrogate the role of TPL2 under genotoxic stress and show TPL2 inhibitor synergizes with the FIRINOX chemotherapy regiment to suppress human and murine in vivo PDAC growth. Lastly, we screened recurrent *MAP3K8* mutations from TCGA and discovered two gain-of-function point mutants, which naturally exist in ovarian cancer and melanoma cell lines, and are highly sensitive to TPL2 blockade.

RESULTS

IRAK signaling dictates NF-κB activity in PDAC and is essential for RAS-oncogenesis

Aberrant NF-κB activation is conventionally defined by increased RELA (or p65 NF-κB family member) expression or nuclear translocation by immunohistochemistry (IHC) in tumor samples (17, 18). To more comprehensively understand the NF-κb associated transcriptomes in PDAC, we evaluated the expression pattern of 37 core NF-κB genes, which include *RELA* as defined by the MSigDB(19), in PDAC samples from TCGA (Firehose Legacy, *n*=185). By unsupervised clustering we observed heterogenous expression of these 37 genes across all samples, reflecting the complexity of mechanisms that activate NF-κB and presence of different categories of NF-κB signatures in PDAC **(Supplementary Figure 1A)**. Because RELA expression is the single, most established NF-κB marker associated with poor prognosis in PDAC, we divided these samples into three groups based on *RELA* mRNA level: $RELA^{High}$ (*z*-score > 1.0, *n* = 29), $RELA^{Med}$ (*z*-score between -1.0 and 1.0, *n* = 129), and $RELA^{Low}$ (*z*-score < -1.0, *n* = 29) (**Figure 1A**). Compared to $RELA^{Low}$ group, patients in $RELA^{High}$ and $RELA^{Med}$ groups had significantly worse progression-free and overall survival (**Figure 1B, Supplementary Figure 1B**). We focused our analysis on $RELA^{High}$ and $RELA^{Low}$ cohorts in order to discern the remaining NF-κB genes that cluster

with *RELA* expression. Notably, many genes in the canonical NF-κB pathway were upregulated in the *RELA*^{High} group (**Figure 1C**), such as the IKK isoform genes (*IKBKB, IKBKE, IKBKG*), inhibitory IκB genes (*NFKBIE, NFKBIB)*, *RELB, NFKB2, IRAK1* and *MYD88.* Of these, *MYD88* and *IRAK1* caught our attention because these are known upstream activators of the IKK kinases(20, 21). *MYD88* and *IRAK1* expression positively correlated with each other (**Supplementary Figure 1C**) and *RELA* (**Supplementary Figure 1D**). Notably, patients with high (*z*-score > 1.0) *MYD88* and/or *IRAK1* expression (termed "*MYD88*^{High}, *IRAK1*^{High}") had significantly worse progression-free survival (Log-rank *P* = 0.0020, **Figure 1D**), disease free status (**Figure 1E)**, overall survival (Log-rank *P* = 0.0147, **Figure 1F**) and vital status at the time of data cutoff (**Figure 1G),** compared to patients with low (*z*-score < 1.0) *MYD88* and/or *IRAK1* expression (termed "*MYD88*^{Low}, *IRAK1*^{Low}"). Together, these results demonstrate positive correlation between *MYD88-IRAK* and *RELA* expression, and further support the TLR/IL-1R canonical pathway as the main driving mechanism of NF-κB activity in PDAC that translates into clinical aggressiveness, congruent with published literature (7, 8, 10, 22).

Unlike MYD88 and IRAK1, which function as adaptor proteins, IRAK4 is the *bone fide* kinase that initiates NF-κB signaling and can be targeted(7, 20). Phospho-activation of IRAK4 is associated with higher RELA activity and poor survival of PDAC patients(7). *IRAK4,* though not included in the pre-defined 37-gene MSigDB NF-κB signature, was significantly overexpressed in PDAC compared to normal pancreas (**Figure 1H**). Analysis of the whole TCGA data showed significantly higher *IRAK4* expression in PDAC compared to majority of other cancers (**Supplementary Figure 1E, Supplementary Table 1)**, supporting a pathogenic role of IRAK4 in PDAC.

Both IRAK4 and KRAS can drive NF-κB signaling in PDAC, but their crosstalk has not been investigated. While KRAS oncoprotein can stimulate the non-canonical IKKε through the RalGEF-RalB-TBK1 effector(23) and the canonical IKKα/β through the PI3K-AKT-mTOR effectors(24), IRAK4 utilizes TAK1 kinase to activate IKKβ(12). Therefore, IRAK4 should not be required for KRAS-induced oncogenesis per se. Yet, to test this, we stably expressed pairs of oncogenes including *c-MYC*^{T58A} and *HRAS*^{G12V}, SV40 *T/t* antigens and *HRAS*^{G12V}, or SV40 *T/t* and *KRAS*^{G12V} in wild-type and *Irak4*$^{-/-}$ murine

embryonic fibroblasts (MEFs). Surprisingly, anchorage-independent (AI) growth in soft agar, a classical assay for transformation, is completely abrogated in *IRAK4*$^{-/-}$ MEFs, but this could be fully rescued with re-expression of murine *Irak4* cDNA (**Figure 1I**). Consistently, *Irak4*$^{-/-}$ MEFs expressing oncogenic *HRAS* or *KRAS* failed to form tumors in nude mice (**Figure 1J**). As further confirmation, we employed the CRISPR/Cas9 technique to ablate *IRAK4* in three *KRAS*-transformed cell lines: KP2 (a murine PDAC line originating from a *p48*-Cre; *Tp53*$^{flox/WT}$; LSL-*Kras*^{G12D}, or KPC mouse), a human embryonic kidney (HEK T/tH) line transformed with hTERT, SV40 *T/t* and *KRAS*^{G12V}, and *KRAS*^{G12D}-mutant PANC-1 line. Again, loss of *IRAK4* completely abrogated tumorigenic growth of these lines in nude mice (**Figure 1J**). KP2 cells expressing small guide RNAs against *Irak4* (sg*Irak4*) were severely impaired not only in AI growth, but also 2-dimensional (2D) proliferation (**Figure 1K, Supplementary Figure 1F**), revealing a role of IRAK4 in cell fitness. Similarly, AI growth of KP2 cells was dose-dependently suppressed by PF06650833(25), a selective IRAK4 inhibitor (IRAK4i, **Figure 1L**). To dissect the role of IRAK4 in *KRAS*-mutant human PDAC, we resorted to the HPNE model, an artificial pancreatic ductal epithelial line immortalized with *hTERT* and HPV *E6/E7*. Stable expression of *KRAS*^{G12D} in this line (named HPNE-*KRAS*^{G12D}) completes the malignant transformation, enabling AI growth. We found that ectopic expression of IRAK4 doubled the AI growth of HPNE-*KRAS*^{G12D} cells but had no effect in the untransformed HPNE cells (**Figure 1M**). Notably, treatment with PF06650833 not only reversed the effect of IRAK4 overexpression, but also crippled the AI growth of HPNE-*KRAS*^{G12D}. Together, these studies showed IRAK4 is essential for and cooperates with mutant *RAS* in oncogenic transformation.

IRAK4 is crucial for oncogenic RAS-driven MAPK signaling

To understand the mechanism by which IRAK4 promotes *RAS*-induced transformation, we first performed an unbiased reverse-phase protein array (RPPA) on HPNE-*KRAS*^{G12D} cells stably expressing IRAK4 or empty vector. Compared to vector cells, IRAK4-overexpressing cells exhibited greater than two-fold increase in phosphorylated (p-) FAK, p-ERK, total FAK and FoxM1, which were reversed by IRAK4i treatment (**Figure 2A**). Indeed, various MAPK target proteins were activated by IRAK4 overexpression and conversely suppressed by IRAK4i (**Figure 2B)**. We observed similar changes with

p-p65/RELA (**Supplementary Figure 2A)**, resonating our previous studies(7, 10). As confirmation, overexpression of wild-type, but not kinase-dead IRAK4, enhanced p-ERK in 293T cells by western blots (**Figure 2C**). Next, we performed RNAseq analysis on KP2 cells expressing vector, two different sg*Irak4*, or sg*Irak4* followed by rescue with a murine *Irak4* cDNA (termed "Rescue"; **Supplementary Figure 2B)**. Consistent with our RPPA results, MAPK, ERK and pro-growth gene ontology (GO) signatures were significantly suppressed in *Irak4*-depleted KP2 cells and restored in *Irak4*-rescued cells (**Figure 2D**). As confirmation, western blots showed reduced p-MEK and p-ERK levels in IRAK4-ablated KP2 cells (**Figure 2E**). Various NF-κB signatures were also similarly affected (**Supplementary Figure 2C).** Gene set enrichment analysis (GSEA) showed oncogenic *KRAS* signaling and PDAC signatures to be significantly downregulated following *Irak4* ablation and restored in *Irak4*-rescued cells (**Figure 2F, 2G** and **2H**). In accordance, IRAK4i dose-dependently suppressed MAPK activity in murine PDAC lines, KP2 and KI (derived from a PDX1-Cre; $INK4a^{flox/flox}$; LSL-$KRAS^{G12D}$ mouse), as well as various *KRAS*-mutant patient-derived cell lines (PDCLs) and HPAC line (**Figure 2I, 2J** and **Supplementary Figure 2D**). As further confirmation, IRAK4i dose-dependently reduced SRE (serum response element)-driven luciferase reporter activity in HPAC cells (**Supplementary Figure 2E**) and viability of various *KRAS*-mutant PDAC lines in vitro (**Supplementary Figure 2F**). To clearly establish the role of IRAK4 in *KRAS*-induced MAPK signaling, we utilized two isogenic pairs of cell lines expression empty vector, $KRAS^{G12D}$ (for HPNE) or $KRAS^{G12V}$ (for 293T). As expected, expression of *KRAS* mutants clearly upregulated p-MEK, p-ERK and p-RSK levels, but all these were dose-dependently blocked by IRAK4i (**Figure 2K**). Importantly, expression of activated MEK-mutant (MEK1-5^{DD}) rendered HEK T/tH-$KRAS^{G12V}$ cells approximately 3-fold less sensitive to growth inhibition by IRAK4i (**Supplementary Figure 2G**), positioning IRAK4 upstream of MEK. Besides MAPK pathway, IRAK4i also suppresses p-p105 level in Pa01C, Pa02C, Pa03C and HPAC cells (**Figure 2J, Supplementary Figure 2D**), resonating previous findings that IRAK4 is a driver of NF-κB pathway(7, 16). Intriguingly, we also observed dose-dependent suppression of SRE activity by IKK inhibitor IMD-0354 in HPAC, suggesting a contribution of IKK to MAPK activity in PDAC cells (**Supplementary Figure 2E).** Together, these results establish IRAK4 as a significant contributor to KRAS-induced MAPK signaling.

TPL2 mediates signaling between IRAK4 and MAPK pathway

Next, we investigated the mechanistic link between IRAK4 and MEK. In myeloid cells, IL-1, TNF or LPS activate MEK and ERK through engaging TPL2 kinase (or COT/MAP3K8) (26, 27). We therefore hypothesized that IRAK4 engages TPL2 to activate MEK and ERK. Indeed, ectopic expression of TPL2 in Pa01C and HPAC cells enhanced p-MEK, p-ERK levels, but this effect was blocked by IRAK4i. Notably, the ectopically expressed TPL2 protein existed in an activated state, as determined by a p-TPL2 antibody, and was dose-dependently deactivated by IRAK4i, confirming IRAK4 as the upstream activator of TPL2 (**Figure 3A** and **Supplementary Figure 3A**). In support, ectopic expression of IRAK4 upregulated p-TPL2, p-MEK and p-ERK in 293T cells (**Figure 3B**).

To strengthen the link between IRAK4, TPL2 and MEK, we next performed leading-edge analysis using 15 published TPL2-associated gene signatures from the Broad Institute MSigDB, including significantly downregulated MAPK-related GO signatures identified in *Irak4*-ablated KP2 cells (**Supplementary Table 3**). Ablation of *Irak4* decreased TPL2 (encoded by MAP3K8) expression in majority of gene sets, and importantly low TPL2 expression was closely associated and clustered with low MEK1 expression (**Figure 3C**, **Supplementary Figure 3B**). These data position TPL2 as the signal transducer between IRAK4 and MEK in PDAC. In human PDAC lines, we observed strong, positive correlation between the protein levels of TPL2 and p-ERK (**Figure 3D**, **3E**) by western blots. In human and murine PDAC tumor tissues, IHC analyses showed co-occurrence of p-ERK, TPL2 and p-IRAK4 staining in the neoplastic ductal epithelia, whereas these markers were largely absent in normal ductal epithelia (**Figure 3F**).

High TPL2 expression is poor prognostic in PDAC

We next performed IHC analyses on a panel of 313 PDAC tissue micro-array (TMA) specimens and found strong, significantly positive correlation of H-score, defined by staining area and intensities, between TPL2 and p-IRAK4 (r = 0.56, P < 0.0001, **Figure 4A, 4B**, and **Supplementary Figure 4A, 4B**). Notably, high TPL2 staining correlated with poor overall survival in PDAC patients based on Wilcoxon P

= 0.03, a statistic that gives more weight to early deaths, as typically seen with PDAC patients (**Figure 4C**). From TCGA and GTEx database, *MAP3K8* mRNA expression was significantly higher in PDAC compared to normal pancreas (**Figure 4D**) and majority of other cancer types (**Supplementary Figure 4C, Supplementary Table 2**). Next, using the median overall survival of TCGA PDAC patients (~15.5 months), we divided patients into two groups, short (<15.5 months OS, n = 92) and longer (≥ 15.5 months OS, n = 93) survivors (**Figure 4E**). The short survivors had significantly higher *MAP3K8* expression (**Figure 4F)**. Conversely, high *MAP3K8* expression (arbitrarily defined as z score > 1, $MAP3K8^{high}$, n = *22*) is significantly associated with poorer overall survival compared to low *MAP3K8* expression (z score < 1, "$MAP3K8^{low}$", n = 28, **Figure 4G)**. Together, these complementary studies position TPL2 as the intermediate kinase between IRAK4 and MEK and signify its potential as a therapeutic target warranting further investigation.

TPL2 drives both MAPK and NFκB signaling in PDAC

From GSEA analysis we found $MAP3K8^{high}$ PDAC samples to be enriched for both KRAS and NF-κB signatures (**Figure 5A),** mirroring our findings with IRAK4 (**Figure 2F**) and congruous with a prior report which showed that TPL2 can phospho-activate the p105 NF-κB factor(28). To determine if TPL2 controls MAPK and NF-κB signaling, we treated *KRAS*-mutant PDAC cells with 4-[(3-Chloro-4-fluorophenyl)amino]-6-[(3-pyridinylmethyl)amino]-1,7-naphthyridine-3-carbonitrile, a selective ATP competitive small molecule TPL2 inhibitor (TPL2i) that can suppress LPS-induced TNFα production in human monocytes (29). Treatment with TPL2i dose-dependently suppressed p-MEK and p-ERK levels in multiple *KRAS*-mutant PDAC lines except PANC-1 (**Figure 5B**), and in 293T cells expressing $KRAS^{G12V}$(**Figure 5C**), establishing TPL2 as a contributor to KRAS-induced MAPK activity. Notably, TPL2i dose-dependently blocked p-MEK and p-ERK without affecting p-BRAF (**Figure 5D**), suggesting that TPL2i does not compromise KRAS-RAF interaction and TPL2 activates MEK independent of RAFs. Apart from MAPK, TPL2i also dose-dependently suppressed p-p105, but this did not lead to increased p50 processing. Notably, TPL2i potently suppressed p-p65 at S276 in three out of four cell lines, but not S536 (**Figure 5D, 5E**), consistent with published literature(30). Conversely, ectopic expression of TPL2

dose-dependently increased p-p105, p-MEK and p-ERK levels in 293T cells (**Supplementary Figure 5A**). These results show that TPL2 controls both MAPK and NF-κB cascades in PDAC.

Like the RAF kinases, TPL2 is a MAP3K that activates MEK. However, in RAS-mutant cells, BRAF inhibitors such as PLX-4720 and dabrafenib paradoxically hyperactivates MAPK cascades, which we also observed in *KRAS*-mutant HPAC, MIA Paca-2 and Pa01C cells expressing SRE-driven luciferase reporter **(Figure 5F** and **Supplementary Figure 5B, 5C**). In contrary, TPL2i dose-dependently suppressed SRE reporter activity in all three cell lines to levels matching those of MEK and ERK inhibitors. Notably, MEK inhibitor trametinib unexpectedly enhanced NF-κB reporter activity in PDAC cells, perhaps representing a resistance mechanism underlying the lack of clinical efficacy of MEK inhibitors. On the other hand, TPL2i and IRAK4i dose-dependently suppressed both SRE as well as NF-κB reporter activities in *KRAS*-mutant PDAC cells (**Supplementary Figure 5D**). Notably, neither TPL2i nor IRAK4i suppressed p-MEK and p-ERK in 293T cells transfected with oncogenic *BRAF*^{V600E} (**Supplementary Figure 5E**), or in BxPc-3 PDAC line that harbors an in-frame gain-of-function *BRAF* mutation and wild-type *KRAS* (**Suppl. Fig. 5F**), demonstrating IRAK4 and TPL2 as separate activators of MAPK, other than RAFs, downstream of KRAS.

Supporting an essential role of TPL2 in *KRAS*-induced transformation, TPL2i dose-dependently suppressed 3-dimensional (3D) AI and 2-dimensional (2D) clonogenic growth of HPNE-*KRAS*^{G12D} cells, HEKT/tH-*KRAS*^{G12V}, conventional PDAC lines and PDCLs (**Figure 5G**, **Supplementary Figure 6A**). Knockdown of TPL2 by shRNA (shTPL2) severely impaired HPAC and Pa01C cell proliferation (**Figure 5H**). The subpopulation that eventually re-grew had only partial TPL2 knockdown but yet displayed reduced p-MEK, p-ERK and p-p105 levels (**Figure 5I**) and were markedly impaired in 2D clonogenic growth (**Figure 5J**), and 3D growth as organoids or soft agar colonies (**Figure 5K**, **Supplementary Figure 6B**). Together, these data establish a critical role for TPL2 in PDAC and *KRAS* signaling via supporting both NF-κB and MAPK pathways.

KRAS induces autocrine IL-1β inflammatory signaling to activate IRAK4 and TPL2

Next, we investigated the mechanism by which KRAS activates the IRAK4-TPL2 axis. IRAK4 and TPL2 are typically activated downstream of IL-1, TNFα and Toll-like receptors, and not directly by KRAS. On this assumption, we surveyed the expression of IL-1/β, TNFα/β, IL-1R and all the TLRs by qRT-PCR of HEK T/tH cells expressing an empty vector or *KRAS*^{G12V}. Of all sixteen targets, only *IL1B* mRNA was significantly upregulated (by ~10 fold) in *KRAS*^{G12V}-expressing cells compared to vector control (**Figure 6A**), which we confirmed by IL-1β ELISA of conditioned media (CM) collected from these cells (~120 fold higher in *KRAS*^{G12V}-expressing cells, **Supplementary Figure 7A)**. Furthermore, analysis of oncogenic KRAS signature showed *IL1B* expression was significantly higher in *MAP3K8*^{high} patients (**Figure 6B).** These results suggest autocrine IL-1β is the driver of IRAK4-TPL2 activity in *KRAS*-mutant cells. In support, *KRAS*^{G12V} expression upregulated p-IRAK4, p-TPL2, p-MEK and p-ERK levels in HEK T/tH cells, but all were dose-dependently reversed by treatment with a neutralizing anti-hIL-1β antibody (**Figure 6C**). CM collected from HEK-T/tH *KRAS*^{G12V} cells was able to upregulate p-TPL2, p-IRAK4, p-MEK and p-ERK levels in HEK T/tH cells, but the effect was blunted with neutralizing anti-IL-1β antibody (**Figure 6D**), shRNA knockdown of IL-1R of recipient HEK T/tH cells (**Supplementary Figure 7B** and **7C**), and completely blocked by co-treatment with TPL2i (**Figure 6E**). In support of these data, CM from HEK-T/tH *KRAS*^{G12V} cells stimulated SRE reporter activity of HPAC cells by approximately 3- fold (**Supplementary Figure 7D**) and treatment of HEK T/tH, HPAC and Pa01C cells with recombinant human IL-1β (hIL-1β) upregulated p-IRAK4, p-TPL2, p-MEK, p-ERK and p-RSK (**Figure 6F**, **Supplementary Figure 7E**). Knockdown of IL-1R also blunted upregulation of p-MEK and p-ERK in HEK-T/tH transfected with *KRAS*^{G12V} or *MAP3K8* (TPL2) (**Figure 6G**), with similar effects observed in *KRAS*-mutant Pa01C cells (**Supplementary Figure 7F**). These data establish autocrine IL-1β-IRAK4-TPL2 signaling as a parallel mechanism, apart from RAF kinases, through which KRAS oncoprotein drives MAPK signaling.

We next investigated the mechanism by which KRAS promotes IL-1β production. We treated HEK T/tH *KRAS*^{G12V} cells with MEK (trametinib), ERK (ulixertinib) or PI3K (GDC-0941) inhibitors and found that both MEK and ERK inhibitors significantly abrogated IL-1β production, whereas PI3Ki had no effect (**Supplementary Figure 7G**). This data depicts a model where KRAS oncoprotein utilizes the MAPK

effectors to promote IL-1β production and create an autocrine IL-1β–IL-1R–IRAK4–TPL2–MAPK feedforward loop that amplifies MAPK signaling. From TCGA database, elevated *IL1B* expression associated with poor prognosis in PDAC (**Figure 6H**). mRNA level of TPL2 (*MAP3K8*) moderately (r = 0.36) and strongly (r = 0.5), positively correlated with *IL1B* and *IL1R1*, respectively (**Supplementary Figure 8A** and **8B**). In KP2 cells, CRISPR knockout of *Irak4* led to downregulation of GO signatures associated with IL-1, and re-expression of *Irak4* ("Rescue") significantly restored these signatures (**Supplementary Figure 8C** and **8D**). In these gene sets, TPL2 was present in the leading edge as a core enrichment in an IRAK4-dependent manner (**Supplementary Figure 8E**), again signifying its role in IL-1 and cytokine signaling. Together, these data establish autocrine IL-1R-IRAK4-TPL2 signaling as an essential mechanism hijacked by KRAS that should be therapeutically targeted.

TPL2 inhibition potentiates chemotherapy by curbing MAPK and NF-κB activation

Molecular-targeted therapies have been ineffective in treating PDAC patients. Therefore, it is unlikely that TPL2i or IRAK4i alone will be clinically effective, and combination regimens will need to be developed. Chemotherapy is currently the only effective treatment modality for PDAC, but treatment response is neither universal nor durable(31, 32). Stress-induced NF-κB and MAPK survival signaling are amongst the multiple mechanisms that underlie *de novo* chemoresistance. To this end, we examined whether the IRAK4-TPL2 axis contributes to chemotherapy-induced survival and resistance, which will help formulate a rational combinatorial regimen for in vivo testing. We treated PDAC cells with five chemotherapeutic agents (gemcitabine, paclitaxel, SN-38, 5-FU and oxaliplatin) commonly used in patient care. Of these agents, SN-38, an active metabolite of irinotecan, was the most potent in inducing p-ERK, p-MEK, p-RSK, and notably p-TPL2 and p-IRAK4 across multiple PDAC lines (**Fig. 7A**, **Supplementary Figure 9A**), suggesting IRAK4 and TPL2 may contribute to MAPK activation following genotoxic stress. NF-κB was also induced, as evident by increase in p-p105.

To determine the mechanism that activates these markers, we treated HPAC cells with gemcitabine/paclitaxel or FIRINOX (5-FU/SN-38/oxaliplatin), which mimic clinical regimens, and surveyed changes in expression of the TLRs and IL-1α/β in HPAC cells. Intriguingly, we observed

significantly upregulated expression of *TLR6*, *TLR9* and *IL1A*, but not *IL1B*, upon exposure to either chemotherapy (**Figure 7B**). Survey of two other PDCLs Pa01C and Pa03C showed *TLR9* to be the only gene consistently upregulated following FIRINOX treatment (**Figure 7C**). Importantly, signaling from TLR9 is transmitted exclusively through IRAK4(33). Indeed, proximity ligation assay showed markedly increased TLR9 and p-IRAK4 interaction following treatment of three different PDAC lines with SN-38 (**Figure 7D**), suggesting TLR9 to be the driver of IRAK4 and TPL2 upon chemotherapy exposure. Interestingly, analysis of TCGA data also revealed strong and significant correlation (Pearson $r = 0.49$, $P = 2.61e\text{-}12$) between *TLR9* and *MAP3K8* (TPL2) mRNA expression in PDAC samples (**Supplementary Figure 9B**). Co-treatment with TPL2i significantly attenuated SN-38-induced p-MEK, p-ERK and p-RSK, and increased PARP cleavage in PDAC lines (**Figure 7E**). Gemcitabine-induced p-MEK, p-ERK levels and SRE activity were also suppressible with TPL2i (**Supplementary Figure 9C** and **9D**), suggesting that induction of MAPK activity is not specific to one class of cytotoxic agent. Besides the MAPK cascade, TPL2i additionally suppressed p-p105 in SN-38-treated Pa01C cells (**Supplementary Figure 9E**), making it a more broad-spectrum therapeutic agent than MEKi or ERKi in curbing chemotherapy-induced survival signaling. PDAC cells co-treated with SN38 and TPL2i showed significantly more apoptosis (**Supplementary Figure 9F** and **9G**) by flow cytometric analysis, and completely lost their clonogenicity, an assay that tests emergence of resistant clones (**Figure 7F, Supplementary Figure 10A**). Notably, the combination of TPL2i and SN-38 was synergistic in suppressing PDAC cell growth by the Loewe additivity model (**Supplementary Figure 10B**). Accordingly, the combination of TPL2i and FIRINOX was significantly more efficacious in suppressing in vivo subcutaneous growth of Pa01C tumors compared to either treatment alone (**Figure 7G** and **Supplementary Figure 10C, 10D**), and without incurring noticeable toxicities (**Supplementary Figure 10E**). TPL2i alone was effective in significantly suppressing growth of orthotopic KI tumors in syngeneic FVB/NJ mice. When combined with FIRINOX, the mean tumor burden was seemingly further reduced, with two mice showing no evidence of cancer, although the difference between TPL2i and combo arms did not reach statistical significance probably due to low mouse number per arm (**Figure 7H)**. These results show that targeting TPL2 overcomes genotoxic stress-induced survival signaling and enhances the efficacy of chemotherapy.

***MAP3K8* point mutations, E188K and R442H, hyperactivate MAPK and NF-κB cascades**

Aside from being summoned by oncogenic *RAS* and genotoxic stress, TPL2 is also spontaneously activated by genetic mutations. At basal state, TPL2 protein is bound and inhibited by p105 (NFκB1) and A20-binding inhibitor of NFκB (ABIN-2). Activated IKK complex phosphorylates p105 and prompts its proteolysis to p50, which releases TPL2(34). TPL2 undergoes phosphorylation at S400 residue by IKK and T290 by an unknown kinase to become fully activated, after which it is proteasomally degraded via polyubiquitination at its C-terminus (35-37). Therefore, C-terminally truncated TPL2 is more stable and potent in activating the MAPK pathway(38). Oncogenic truncations and fusions of *MAP3K8* are reported in spitzoid melanomas and predict sensitivity to MEK inhibitors in vitro(39). Besides truncations, from TCGA database we noticed several point mutations in *MAP3K8* across various non-PDAC cancer types that have not been characterized. To this end, we investigated five point-mutants that occur with the highest frequency: E188K, R397H, R442H, L444V, R459W (**Figure 8A**). Of these mutants we found E188K and R442H to be the most potent in stimulating SRE- and NF-κB reporter activities (**Supplementary Figure 11A**, **11B**), which we characterized in further detail. E188K mutation is detected in oligodendroglioma, colon and urothelial carcinoma, whereas R442 can acquire missense (to H/C) or non-sense mutations in colon, ovarian, gastric cancers and rhabdoid tumors.

When expressed at the same level as wild-type, $TPL2^{E188K}$ is markedly more potent in activating MEK, ERK, RSK and p105 (**Figure 8B**), as well as inducing SRE and NF-κB reporter activities (**Figure 8C**) in unperturbed 293T cells, clearly showing this is a gain-of-function mutation. To comprehensively evaluate the impact of E188K mutation, we performed RPPA analysis on 293T cells ectopically expressing vector, and roughly equal amount of $TPL2^{WT}$ or $TPL2^{E188K}$ (**Figure 8B**). Of all 441 markers analyzed, p-ERK is the most differentially upregulated marker in $TPL2^{E188K}$-expressing cells (**Figure 8D**), validating our findings with immunoblots and reporter assay. We also observed significantly increased p-S6, a known substrate of ERK, and p-c-Jun which has been described as a TPL2 effector(30) (**Figure 8E**). This analysis showed, in a comprehensive unbiased manner, MEK-ERK cascade to be the predominantly signaling cascade activated by E188K mutation.

To delineate the molecular mechanism underlying the enhanced kinase activity of TPL2^{E188K}, we first compared the half-lives of TPL2^{WT} and TPL2^{E188K} in 293T cells treated with a protein synthesis inhibitor, cycloheximide. Surprisingly, we found that the E188K mutation, despite located within the kinase domain, rendered TPL2 protein more stable (**Figure 9A**). Supporting this finding, immunoprecipitation assay showed E188K mutation almost completely abolished TPL2 polyubiquitination, a prerequisite for proteasomal degradation (**Figure 9B**). To evaluate the oncogenicity of TPL2^{E188K}, we obtained Hs695T, a *BRAF*^{V600E}-mutant melanoma cell line that naturally harbors a *MAP3K8*^{E188K} mutation. Sanger sequencing of cDNA from Hs695T confirmed a G→A mutation in codon 188 of *MAP3K8*, which converts glutamate (GAG) to lysine (AAG) (**Figure 9C**). We therefore speculate that TPL2^{E188K} may be a oncoprotein driving MAPK activation in this cell line. Supporting this notion, treatment with TPL2i inhibition suppressed p-ERK and p-MEK (**Figure 9D)** as well as in vitro proliferation and viability of Hs695T cells (**Figure 9E** and **Supplementary Figure 11C**). Importantly, BRAF inhibitor PLX4032 had modest growth suppressive effect but when combined with TPL2, it significantly lowered the viability of Hs695T (**Figure 9F**), indicating that both *BRAF* and *MAP3K8* mutations contribute to MAPK activity in this cell line.

We next determined the effect of mutation at codon 442, which resides in the C-terminus, implying disruption of degradation function. We chose to study the R442H mutant because it is the most common mutation described in TCGA and more potent in induced SRE and NF-κB reporter activity than wild-type protein (**Supplementary Figure 11A** and **11B**). Compared to TPL2^{WT}, TPL2^{R442H} is more potent in activating MEK, ERK and RSK (**Figure 10A**) when expressed at equal levels. As expected, the stability of TPL2^{R442H} mutant protein was higher than TPL2^{WT} and comparable to C-terminally truncated TPL2 (**Figure 10B**). Interestingly, other mutations including L444V and R459W also render TPL2 slightly more stable than the wild-type form, albeit not to the degree imparted by R442H. All these mutations reduce polyubiquitination of TPL2 (**Figure 10C**), which explains their increased stability. Naturally occurring *MAP3K8*^{R442H} mutation is reported in an ovarian cancer cell line IGROV-1(40). Remarkably, short duration (2 hours) treatment with very low dose of TPL2i (1μM) completely blocked p-MEK, p-ERK and p-RSK in this cell line to undetectable levels even with high exposure time (**Figure 10D**), suggesting that TPL2 is the dominant driver of MAPK activity in this cell line. In support, partial knockdown of TPL2 also reduced

MAPK activity in IGROV-1 (**Figure 10E**). Pharmacologic inhibition or silencing of TPL2i significantly decreased the proliferation, colony forming ability and AI growth of IGROV-1 (**Figure 10F, 10G** and **Supplementary Figure 12A-C**), consistent with prior reports(41). Importantly, while knockdown of TPL2 markedly crippled the ability of IGROV-1 to grow into 3D organoids or 2D clones, these growths could only be rescued by re-expression of $TPL2^{R442H}$ but not $TPL2^{WT}$ (**Figure 10H, Supplementary Figure 12D**). Overall, these studies are the first to describe gain-of-function point mutations of *MAP3K8* (TPL2) in human cancers, further prompting the need to identify these mutations in clinical practice and develop dedicated TPL2 inhibitor for clinical trials.

DISCUSSION

Our present study provides broader understanding of the role of IRAK4-TPL2 in human cancers. Using genetically-defined artificial cell lines and PDAC as disease model, we show that KRAS oncoprotein utilizes the MAPK cascade to upregulate IL-1β production, leading to autocrine activation of the IRAK4-TPL2, which feeds back to escalate MAPK activity and additionally the NF-κB cascade. Following genotoxic stress, PDAC cells upregulate TLR9, leading to enhanced utilization of IRAK4-TPL2 axis to sustain survival. Additionally, we characterize what we believe to be novel gain-of-function TPL2 mutations that hyperactivate the MAPK and NF-κB pathways.

The malignant feats of RAS oncoproteins result from direct and indirect signaling mechanisms. RAS oncoproteins can directly bind and activate several effectors including the RAF kinases, PI3 kinases, RalGEFs and Tiam1(2). Through these pathways, a plethora of inflammatory chemokines and cytokines including IL-6, IL-8, IL-1α/β and CCL5 are produced, which in an autocrine manner trigger the inflammatory JAK/STAT and NF-κB cascades(10, 22, 42-46). These secondary events not only help propagate tumor progression, but also shield cancer cells from therapeutic attacks. For instance, in *KRAS*-mutant lung cancer, TBK1 and IKKε-driven CCL5 and IL-6 can activate the JAK/STAT pathway to confer resistance to MEK inhibitors(42). In PDAC, STAT3 activation drives resistance to MEK inhibitor (44, 45). Therefore, autocrine/paracrine cytokine signaling provides equally essential support, in addition

to the intrinsic oncogenic events, that help cancer cells adapt and withstand stress. In this study, we show autocrine IL-1β-driven IRAK4-TPL2 axis to be an essential component of KRAS and MAPK signaling. Because IRAK4 is typically activated by inflammatory receptors IL-1R, TLRs and TNFR, it is most widely studied as the driver of NF-κB activity in immune cells(47). Strikingly, ablation of IRAK4 completely blocked RAS-induced transformation and tumorigenicity in both epithelial cells and fibroblasts, as well as PDAC cells. These data are in strong agreement with an elegant study by Ling et al. that ablation of IKKβ, a key downstream substrate of IRAK4, completely abolished PDAC development in *KRAS/Ink4a* mouse model(8). IL-1R antagonist, Anakinra is currently being tested in clinical trial in combination with chemotherapy for PDAC (NCT02550327). Downstream of IRAK4, we revealed TPL2 as a MAP3K that drives MEK-ERK and p105 NF-κB in *KRAS*-mutant cells independent of the RAF kinases. Therefore, TPL2 is a promising therapeutic target that controls multiple signaling cascades in *KRAS*-driven cancers.

Aside from enforcing KRAS autocrine signaling, the IRAK4-TPL2 axis is further utilized following genotoxic stress as a survival mechanism. Induction of MAPK activity is a well-established mechanism that allows cancer cells to endure genotoxic stress (48). However, MEK inhibitors fail to potentiate chemotherapy in pancreatic cancer(49, 50), suggesting that targeting MAPK alone is insufficient, or that compensatory escape mechanisms, such as enhanced NF-κB activity should be co-targeted. Similarly, in a prostate cancer model, addition of NF-κB pathway inhibitor significantly potentiates the anti-tumor effect of MEK inhibitors(51). Here in our study, we found that PDAC cells adapt to chemotherapy by upregulating TLR9, which signals through IRAK4-IKK-TPL2 to activate multiple pathways. Therefore, PDAC cells utilize different receptors, IL-1R at baseline and TLR9 during genotoxic stress, to engage the same IRAK4-IKK-TPL2 axis for survival. It is important to keep in mind that since the therapeutic spectrum of TPL2i extends beyond MEK-ERK, encompassing the NF-κB, JNK and p38 cascades, all of which have been implicated in chemoresistance, TPL2 may be a more promising therapeutic target than MEK or ERK when combined with chemotherapy, at least in PDAC. In accordance, pharmacologic TPL2 inhibition completely blocked chemotherapy induced MAPK and NF-κB activation, resulting in greater apoptosis and tumor suppression in vivo (**Supplementary Figure 9, 10** and **13**).

To our best knowledge, our study is the first to report gain-of-function point mutations of TPL2. Overexpression, C-terminal truncations, or fusions of TPL2 have been found in T-cell neoplasms, melanoma, ovarian, breast and lung cancers. These mutations are associated with RAF inhibitor resistance, and can be targeted with MEK inhibitors(39, 41, 52-55). Compared to wild-type protein, E188K and R442H mutants we studied are more stable and capable of hyperactivating both MAPK and NF-κB cascades. Furthermore, cancer cell lines naturally harboring these mutations (Hs695T for E188K, and IGROV1 for R442H) are highly sensitive to TPL2 inhibition. Importantly, TPL2 inhibitor significantly suppressed MAPK activity and proliferation of *BRAF*^{V600E}*/MAP3K8*^{E188K} double mutant Hs695T cells, but not in *BRAF*^{V600E}*/MAP3K8*^{WT} BxPc-3 cells, demonstrating that *MAP3K8*^{E188K} is oncogenic.

The crystal structure of the C-terminus of TPL2 has not been resolved, and therefore how these mutations conformationally alter the entire protein is unclear. It has been suggested that the C-terminus of TPL2 negatively regulates TPL2 kinase activity via intramolecular interaction with its kinase domain(38). In addition, the C-terminus of TPL2, upon IKK dependent phosphorylation of S400 and S443, binds to 14-3-3 complex that stabilizes TPL2 and increases its kinase activity towards MEK1, possibly by relieving the kinase inhibitory interaction between the C-terminus and kinase domain(35). The R442H mutation may impact TPL2 binding with 14-3-3, resulting in the increased stability and increased MEK and ERK activation that we observed in our experiments. On the other hand, R442 is part of a conserved MAPK recognition motif (KRQRSLYIDL) present on TPL2(39). This raises the possibility that mutation of Arg to His at this residue may alter TPL2 binding affinity and/or specificity towards substrates, although detailed additional work is required to prove this. The mechanism by which E188K mutation stabilizes the protein is intriguing, as this residue is located within the kinase domain which is distant from the C-terminal degron. It is possible that this E188K mutation enhances the intrinsic kinase activity in addition to disrupting its degradation, but this will require resolution of the entire TPL2 protein structure. Furthermore, mechanism including the E3 ligase that governs the degradation of TPL2 is unknown and should be investigated. This is especially important because our PDAC TMA showed p-IRAK4 level to be strongly associated with high TPL2 protein level, which in turn is associated with poor prognosis. Therefore, we speculate that high IRAK4 activity may protect TPL2 from degradation, although the

detailed mechanism remains to be determined. Whether upstream TLR/IL-1R activation is required for the enhanced activity of E188K or R442H mutants is uncertain. However, this is unlikely since these mutants exhibit markedly enhanced activity in unperturbed 293T cells compared to the wild-type counterpart. Importantly, both E188K and R442H mutants remain sensitive to the TPL2i that we tested. TPL2i and RAFi cooperate to curb the growth of Hs695T cells which harbor *MAP3K8*^{E188K} and *BRAF*^{V600E} mutation, and MAPK activity in IGROV1 ovarian cancer cells that harbor only the *MAP3K8*^{R442H} mutation is completely abolished by low dose TPL2i.

In this study we demonstrated the in vivo anti-tumor efficacy of TPL2i as a single agent and in combination with chemotherapy. Targeting IRAK4 or TPL2 are not expected to have severe side effects and none were observed in mice. *Irak4* knocked out mice are viable and have normal lifespan but are immunocompromised(33). Humans with inborn *IRAK4*-deficiency are susceptible to life-threatening bacterial infection in early infancy, but with proper antibiotic prophylaxis have survived into adolescence and adulthood (56). IRAK4 inhibitor CA-4948 is now in clinical trial (NCT03328078) for patients with refractory hematologic malignancies, and is found to be rather well-tolerated, with 23% of patients developing Grade 1~2 neutropenia (57). Similarly, *Map3k8* knockout mice do not exhibit obvious phenotypic defects, and have normal bone marrow but are impaired in MEK-ERK activation and TNFα production following LPS challenge(58). To date, no TPL2 inhibitor has been developed for and tested in clinical trials. We argue TPL2 is a more versatile kinase that controls multiple oncogenic pathways besides MEK-ERK, and therefore development of a dedicated TPL2 inhibitor is needed especially for *KRAS*- or *MAP3K8*-mutant cancers.

In conclusion, our study comprehensively describes an essential role of IRAK4 and TPL2 in oncogenic RAS signaling, using PDAC as disease model. Mechanistically, we show that the IRAK4-TPL2 axis is differentially engaged at basal-state versus during genotoxic stress by different upstream receptors. We show TPL2 inhibition synergistically sensitizes PDAC to chemotherapy in in vivo models, which we propose is a novel therapeutic strategy. Finally, we characterize two gain-of-function mutations of *MAP3K8* (TPL2) in melanoma and ovarian cancer, which complement other studies describing overexpression, truncations, or fusion of *MAP3K8* (TPL2) as being oncogenic. Overall, our study urges

development of dedicated TPL2 inhibitors and detection of *MAP3K8* (TPL2) mutations for cancer patients.

METHODS (Additional methods description can be found in Supplementary Data)

Cell lines

All cell lines including HPNE, HPNE-*KRAS*^{G12D}, HPAC, Hs695T, were obtained from ATCC, which performed its own authentication by short tandem repeat DNA profiling. IGROV1 cells were a kind gift from Dr. Katherine Fuh (Washington University, St. Louis, USA), originated from the NCI-60 panel(59) and not further authenticated. The HEK T/tH cell line was a gift from Dr. Christopher Counter (Duke University, Durham, USA) and previously published(60). KP2 cell line was a gift from Dr. David DeNardo (Washington University, St. Louis, USA) and authenticated by whole-exome sequencing (61). Murine embryonic fibroblasts (MEFs) were isolated from wild-type or *IRAK4-null* mice as described (62). The patient-derived cell lines, Pa01C, Pa02C, Pa03C, Pa04C, Pa14C and Pa16C were a kind gift from Dr. Channing J. Der (University of North Carolina, Chapel Hill, USA) and have been described (63). All cell lines were cultured in DMEM supplemented with 10% fetal bovine serum and 1% penicillin/streptomycin except IGROV1 and Hs695T which were cultured in RPMI-1640 and MEM with nonessential amino-acids respectively, along with other supplements stated above. Mycoplasma testing was performed annually using MycoSEQ Detection kit (Applied Biosystems). All lines were used for fewer than 6 months after receipt or resuscitation from cryopreservation. For all drug treatments, when applicable concentration of 0 (zero) or “V” is treatment with vehicle, DMSO.

In vivo tumorigenesis assays

All animal experiments were conducted under approval by IACUC protocol (#20190138). For subcutaneous xenograft, approximately 5 million cells per flank were implanted into 6-week-old athymic nude mice (NU/J, Jackson Laboratory). When applicable, treatment with drug compound was initiated

when tumors were palpable. FIRINOX (25mg kg^{-1} 5-fluorouracil, 17.5mg kg^{-1} irinotecan and 3.35mg kg^{-1} oxaliplatin) was administered via intraperitoneal injection weekly in 50μL PBS. TPL2i was administered by intraperitoneal injection at 10mg kg^{-1} in 40μL DMSO, 5 days a week. Mice in control group were treated with vehicle. Tumor volume was calculated as $(width^2) \times (length \times 0.5)$. Tumors were measured and mice were weighed three days a week. For orthotopic implantation, murine KI PDAC cells were injected into the pancreas of 7-week-old female FVB/NJ mice (Jackson Laboratory) as previously described (64). 6 days after implantation, treatment with vehicle, FIRINOX (same dose as above), or TPL2i (30mg kg^{-1}) was initiated for 14 days at which time all mice were sacrificed. In vivo tumor progression was monitored using ultrasound (VScan, GE Healthcare) with final day representative tumor images shown.

Statistical Analyses

All results, when applicable, are expressed as mean ± SEM. Statistical analysis was performed using the GraphPad Prism v7/8 software. Unpaired student's two-tailed(two-sided) t-tests were used to compare two groups when appropriate. For multiple groups, one-way or two-way ANOVA analysis with appropriate post-test were used. In instances of systemic/group variation, repeated measures ANOVA was utilized. Unadjusted P values < 0.05 were considered statistically significant. Adjusted P value metrics are stated at end of each figure legend where applicable. Cox proportional hazards models were used to evaluate the relationships between clinical characteristics and overall survival. Kaplan-Meier curve was generated using SAS version 9.4 (SAS Institute, Cary, NC) and analysed by log rank tests.

Study Approvals

The Washington University PDAC Tissue Micro-Array (TMA) was IRB approved (#201404143) and published (65). Patient consent was waived per IRB approval. All studies were performed per ethical principles of Declaration of Helsinki. All animal (mouse) experiments were conducted under IACUC approval (#20190138).

Data Availability

RNAseq data on KP2 WT, *Irak4*-knockout and rescue cells is deposited in GEO, accession number GSE148442.

AUTHOR CONTRIBUTIONS

PBD and KHL developed the concept, designed the experiments, and wrote the manuscript. PBD performed most experiments, completed all revisions, and acquired and analyzed most of the data. NK, DZ, HJ, YC and LL each contributed one or more panels of data in the manuscript. QW, PMG and KS provided technical assistance. AWG generated human PDAC TMA. KHL assigned author responsibilities, supervised, provided funding and administered the project.

ACKNOWLEDGEMENT

This study was supported by NIH (R37CA219697-01), WUSTL SPORE Career Enhancement Award grant (1P50CA196510-01A1), American Cancer Society (RSG-17-203-01-TBG), and Alvin J. Siteman Cancer Center Siteman Investment Program (supported by Barnard Trust and The Foundation for Barnes-Jewish Hospital). We acknowledge the WUSTL DDRCC (grant P30 DK052574) for providing technical support. The content is solely the responsibility of the authors and does not necessarily represent the official view of the NIH.

REFERENCES

1. Canon J, Rex K, Saiki AY, Mohr C, Cooke K, Bagal D, Gaida K, Holt T, Knutson CG, Koppada N, et al. The clinical KRAS(G12C) inhibitor AMG 510 drives anti-tumour immunity. *Nature.* 2019;575(7781):217-23
2. Waters AM, and Der CJ. KRAS: The Critical Driver and Therapeutic Target for Pancreatic Cancer. *Cold Spring Harb Perspect Med.* 2018;8(9):a031435
3. Chung V, McDonough S, Philip PA, Cardin D, Wang-Gillam A, Hui L, Tejani MA, Seery TE, Dy IA, Al Baghdadi T, et al. Effect of Selumetinib and MK-2206 vs Oxaliplatin and Fluorouracil in Patients With Metastatic Pancreatic Cancer After Prior Therapy: SWOG S1115 Study Randomized Clinical Trial. *JAMA Oncol.* 2017;3(4):516-22
4. Algul H, Adler G, and Schmid RM. NF-kappaB/Rel transcriptional pathway: implications in pancreatic cancer. *Int J Gastrointest Cancer.* 2002;31(1-3):71-8
5. Wang W, Abbruzzese JL, Evans DB, Larry L, Cleary KR, and Chiao PJ. The nuclear factor-kappa B RelA transcription factor is constitutively activated in human pancreatic adenocarcinoma cells. *Clin Cancer Res.* 1999;5(1):119-27
6. Prabhu L, Mundade R, Korc M, Loehrer PJ, and Lu T. Critical role of NF-kappaB in pancreatic cancer. *Oncotarget.* 2014;5(22):10969-75
7. Zhang D, Li L, Jiang H, Knolhoff BL, Lockhart AC, Wang-Gillam A, DeNardo DG, Ruzinova MB, and Lim KH. Constitutive IRAK4 Activation Underlies Poor Prognosis and Chemoresistance in Pancreatic Ductal Adenocarcinoma. *Clin Cancer Res.* 2017;23(7):1748-59
8. Ling J, Kang Y, Zhao R, Xia Q, Lee DF, Chang Z, Li J, Peng B, Fleming JB, Wang H, et al. KrasG12D-induced IKK2/beta/NF-kappaB activation by IL-1alpha and p62 feedforward loops is required for development of pancreatic ductal adenocarcinoma. *Cancer Cell.* 2012;21(1):105-20
9. Prescott JA, and Cook SJ. Targeting IKKbeta in Cancer: Challenges and Opportunities for the Therapeutic Utilisation of IKKbeta Inhibitors. *Cells.* 2018;7(9):115
10. Zhang D, Li L, Jiang H, Li Q, Wang-Gillam A, Yu J, Head R, Liu J, Ruzinova MB, and Lim KH. Tumor-Stroma IL1beta-IRAK4 Feedforward Circuitry Drives Tumor Fibrosis, Chemoresistance, and Poor Prognosis in Pancreatic Cancer. *Cancer Res.* 2018;78(7):1700-12
11. Jain A, Kaczanowska S, and Davila E. IL-1 Receptor-Associated Kinase Signaling and Its Role in Inflammation, Cancer Progression, and Therapy Resistance. *Front Immunol.* 2014;5(553
12. Lim KH, and Staudt LM. Toll-like receptor signaling. *Cold Spring Harb Perspect Biol.* 2013;5(1):a011247
13. Srivastava R, Geng D, Liu Y, Zheng L, Li Z, Joseph MA, McKenna C, Bansal N, Ochoa A, and Davila E. Augmentation of therapeutic responses in melanoma by inhibition of IRAK-1,-4. *Cancer Res.* 2012;72(23):6209-16
14. Wee ZN, Yatim SM, Kohlbauer VK, Feng M, Goh JY, Bao Y, Lee PL, Zhang S, Wang PP, Lim E, et al. IRAK1 is a therapeutic target that drives breast cancer metastasis and resistance to paclitaxel. *Nat Commun.* 2015;6(8746
15. Adams AK, Bolanos LC, Dexheimer PJ, Karns RA, Aronow BJ, Komurov K, Jegga AG, Casper KA, Patil YJ, Wilson KM, et al. IRAK1 is a novel DEK transcriptional target and is essential for head and neck cancer cell survival. *Oncotarget.* 2015;6(41):43395-407
16. Li Q, Chen Y, Zhang D, Grossman J, Li L, Khurana N, Jiang H, Grierson PM, Herndon J, DeNardo DG, et al. IRAK4 mediates colitis-induced tumorigenesis and chemoresistance in colorectal cancer. *JCI Insight.* 2019;4(19):e130867

17. Weichert W, Boehm M, Gekeler V, Bahra M, Langrehr J, Neuhaus P, Denkert C, Imre G, Weller C, Hofmann HP, et al. High expression of RelA/p65 is associated with activation of nuclear factor-kappaB-dependent signaling in pancreatic cancer and marks a patient population with poor prognosis. *Br J Cancer.* 2007;97(4):523-30
18. Fujioka S, Sclabas GM, Schmidt C, Frederick WA, Dong QG, Abbruzzese JL, Evans DB, Baker C, and Chiao PJ. Function of nuclear factor kappaB in pancreatic cancer metastasis. *Clin Cancer Res.* 2003;9(1):346-54
19. Liberzon A, Birger C, Thorvaldsdottir H, Ghandi M, Mesirov JP, and Tamayo P. The Molecular Signatures Database (MSigDB) hallmark gene set collection. *Cell Syst.* 2015;1(6):417-25
20. Lin SC, Lo YC, and Wu H. Helical assembly in the MyD88-IRAK4-IRAK2 complex in TLR/IL-1R signalling. *Nature.* 2010;465(7300):885-90
21. Adachi O, Kawai T, Takeda K, Matsumoto M, Tsutsui H, Sakagami M, Nakanishi K, and Akira S. Targeted disruption of the MyD88 gene results in loss of IL-1- and IL-18-mediated function. *Immunity.* 1998;9(1):143-50
22. Zhuang Z, Ju HQ, Aguilar M, Gocho T, Li H, Iida T, Lee H, Fan X, Zhou H, Ling J, et al. IL1 Receptor Antagonist Inhibits Pancreatic Cancer Growth by Abrogating NF-kappaB Activation. *Clin Cancer Res.* 2016;22(6):1432-44
23. Chien Y, Kim S, Bumeister R, Loo YM, Kwon SW, Johnson CL, Balakireva MG, Romeo Y, Kopelovich L, Gale M, Jr., et al. RalB GTPase-mediated activation of the IkappaB family kinase TBK1 couples innate immune signaling to tumor cell survival. *Cell.* 2006;127(1):157-70
24. Dan HC, Cooper MJ, Cogswell PC, Duncan JA, Ting JP, and Baldwin AS. Akt-dependent regulation of NF-{kappa}B is controlled by mTOR and Raptor in association with IKK. *Genes Dev.* 2008;22(11):1490-500
25. Lee KL, Ambler CM, Anderson DR, Boscoe BP, Bree AG, Brodfuehrer JI, Chang JS, Choi C, Chung S, Curran KJ, et al. Discovery of Clinical Candidate 1-{[(2S,3S,4S)-3-Ethyl-4-fluoro-5-oxopyrrolidin-2-yl]methoxy}-7-methoxyisoquinoli ne-6-carboxamide (PF-06650833), a Potent, Selective Inhibitor of Interleukin-1 Receptor Associated Kinase 4 (IRAK4), by Fragment-Based Drug Design. *J Med Chem.* 2017;60(13):5521-42
26. Mielke LA, Elkins KL, Wei L, Starr R, Tsichlis PN, O'Shea JJ, and Watford WT. Tumor progression locus 2 (Map3k8) is critical for host defense against Listeria monocytogenes and IL-1 beta production. *J Immunol.* 2009;183(12):7984-93
27. Pattison MJ, Mitchell O, Flynn HR, Chen CS, Yang HT, Ben-Addi H, Boeing S, Snijders AP, and Ley SC. TLR and TNF-R1 activation of the MKK3/MKK6-p38alpha axis in macrophages is mediated by TPL-2 kinase. *Biochem J.* 2016;473(18):2845-61
28. Babu GR, Jin W, Norman L, Waterfield M, Chang M, Wu X, Zhang M, and Sun SC. Phosphorylation of NF-kappaB1/p105 by oncoprotein kinase Tpl2: implications for a novel mechanism of Tpl2 regulation. *Biochim Biophys Acta.* 2006;1763(2):174-81
29. Gavrin LK, Green N, Hu Y, Janz K, Kaila N, Li HQ, Tam SY, Thomason JR, Gopalsamy A, Ciszewski G, et al. Inhibition of Tpl2 kinase and TNF-alpha production with 1,7-naphthyridine-3-carbonitriles: synthesis and structure-activity relationships. *Bioorg Med Chem Lett.* 2005;15(23):5288-92
30. Das S, Cho J, Lambertz I, Kelliher MA, Eliopoulos AG, Du K, and Tsichlis PN. Tpl2/cot signals activate ERK, JNK, and NF-kappaB in a cell-type and stimulus-specific manner. *J Biol Chem.* 2005;280(25):23748-57
31. Conroy T, Desseigne F, Ychou M, Bouche O, Guimbaud R, Becouarn Y, Adenis A, Raoul JL, Gourgou-Bourgade S, de la Fouchardiere C, et al. FOLFIRINOX versus

gemcitabine for metastatic pancreatic cancer. *The New England journal of medicine.* 2011;364(19):1817-25

32. Von Hoff DD, Ervin T, Arena FP, Chiorean EG, Infante J, Moore M, Seay T, Tjulandin SA, Ma WW, Saleh MN, et al. Increased survival in pancreatic cancer with nab-paclitaxel plus gemcitabine. *The New England journal of medicine.* 2013;369(18):1691-703
33. Suzuki N, Suzuki S, Duncan GS, Millar DG, Wada T, Mirtsos C, Takada H, Wakeham A, Itie A, Li S, et al. Severe impairment of interleukin-1 and Toll-like receptor signalling in mice lacking IRAK-4. *Nature.* 2002;416(6882):750-6
34. Beinke S, Robinson MJ, Hugunin M, and Ley SC. Lipopolysaccharide activation of the TPL-2/MEK/extracellular signal-regulated kinase mitogen-activated protein kinase cascade is regulated by IkappaB kinase-induced proteolysis of NF-kappaB1 p105. *Mol Cell Biol.* 2004;24(21):9658-67
35. Ben-Addi A, Mambole-Dema A, Brender C, Martin SR, Janzen J, Kjaer S, Smerdon SJ, and Ley SC. IkappaB kinase-induced interaction of TPL-2 kinase with 14-3-3 is essential for Toll-like receptor activation of ERK-1 and -2 MAP kinases. *Proc Natl Acad Sci U S A.* 2014;111(23):E2394-403
36. Roget K, Ben-Addi A, Mambole-Dema A, Gantke T, Yang HT, Janzen J, Morrice N, Abbott D, and Ley SC. IkappaB kinase 2 regulates TPL-2 activation of extracellular signal-regulated kinases 1 and 2 by direct phosphorylation of TPL-2 serine 400. *Mol Cell Biol.* 2012;32(22):4684-90
37. Cho J, Melnick M, Solidakis GP, and Tsichlis PN. Tpl2 (tumor progression locus 2) phosphorylation at Thr290 is induced by lipopolysaccharide via an Ikappa-B Kinase-beta-dependent pathway and is required for Tpl2 activation by external signals. *J Biol Chem.* 2005;280(21):20442-8
38. Ceci JD, Patriotis CP, Tsatsanis C, Makris AM, Kovatch R, Swing DA, Jenkins NA, Tsichlis PN, and Copeland NG. Tpl-2 is an oncogenic kinase that is activated by carboxy-terminal truncation. *Genes Dev.* 1997;11(6):688-700
39. Newman S, Fan L, Pribnow A, Silkov A, Rice SV, Lee S, Shao Y, Shaner B, Mulder H, Nakitandwe J, et al. Clinical genome sequencing uncovers potentially targetable truncations and fusions of MAP3K8 in spitzoid and other melanomas. *Nat Med.* 2019;25(4):597-602
40. Ghandi M, Huang FW, Jane-Valbuena J, Kryukov GV, Lo CC, McDonald ER, 3rd, Barretina J, Gelfand ET, Bielski CM, Li H, et al. Next-generation characterization of the Cancer Cell Line Encyclopedia. *Nature.* 2019;569(7757):503-8
41. Gruosso T, Garnier C, Abelanet S, Kieffer Y, Lemesre V, Bellanger D, Bieche I, Marangoni E, Sastre-Garau X, Mieulet V, et al. MAP3K8/TPL-2/COT is a potential predictive marker for MEK inhibitor treatment in high-grade serous ovarian carcinomas. *Nat Commun.* 2015;6(8583
42. Zhu Z, Aref AR, Cohoon TJ, Barbie TU, Imamura Y, Yang S, Moody SE, Shen RR, Schinzel AC, Thai TC, et al. Inhibition of KRAS-driven tumorigenicity by interruption of an autocrine cytokine circuit. *Cancer Discov.* 2014;4(4):452-65
43. Ancrile BB, O'Hayer KM, and Counter CM. Oncogenic ras-induced expression of cytokines: a new target of anti-cancer therapeutics. *Mol Interv.* 2008;8(1):22-7
44. Nagathihalli NS, Castellanos JA, Lamichhane P, Messaggio F, Shi C, Dai X, Rai P, Chen X, VanSaun MN, and Merchant NB. Inverse Correlation of STAT3 and MEK Signaling Mediates Resistance to RAS Pathway Inhibition in Pancreatic Cancer. *Cancer Res.* 2018;78(21):6235-46

45. Nagathihalli NS, Castellanos JA, Shi C, Beesetty Y, Reyzer ML, Caprioli R, Chen X, Walsh AJ, Skala MC, Moses HL, et al. Signal Transducer and Activator of Transcription 3, Mediated Remodeling of the Tumor Microenvironment Results in Enhanced Tumor Drug Delivery in a Mouse Model of Pancreatic Cancer. *Gastroenterology.* 2015;149(7):1932-43 e9
46. Ancrile B, Lim KH, and Counter CM. Oncogenic Ras-induced secretion of IL6 is required for tumorigenesis. *Genes Dev.* 2007;21(14):1714-9
47. Senger K, Pham VC, Varfolomeev E, Hackney JA, Corzo CA, Collier J, Lau VWC, Huang Z, Hamidzhadeh K, Caplazi P, et al. The kinase TPL2 activates ERK and p38 signaling to promote neutrophilic inflammation. *Sci Signal.* 2017;10(475)
48. Salaroglio IC, Mungo E, Gazzano E, Kopecka J, and Riganti C. ERK is a Pivotal Player of Chemo-Immune-Resistance in Cancer. *Int J Mol Sci.* 2019;20(10):2505
49. Infante JR, Somer BG, Park JO, Li CP, Scheulen ME, Kasubhai SM, Oh DY, Liu Y, Redhu S, Steplewski K, et al. A randomised, double-blind, placebo-controlled trial of trametinib, an oral MEK inhibitor, in combination with gemcitabine for patients with untreated metastatic adenocarcinoma of the pancreas. *Eur J Cancer.* 2014;50(12):2072-81
50. Van Cutsem E, Hidalgo M, Canon JL, Macarulla T, Bazin I, Poddubskaya E, Manojlovic N, Radenkovic D, Verslype C, Raymond E, et al. Phase I/II trial of pimasertib plus gemcitabine in patients with metastatic pancreatic cancer. *Int J Cancer.* 2018;143(8):2053-64
51. Gioeli D, Wunderlich W, Sebolt-Leopold J, Bekiranov S, Wulfkuhle JD, Petricoin EF, 3rd, Conaway M, and Weber MJ. Compensatory pathways induced by MEK inhibition are effective drug targets for combination therapy against castration-resistant prostate cancer. *Mol Cancer Ther.* 2011;10(9):1581-90
52. Johannessen CM, Boehm JS, Kim SY, Thomas SR, Wardwell L, Johnson LA, Emery CM, Stransky N, Cogdill AP, Barretina J, et al. COT drives resistance to RAF inhibition through MAP kinase pathway reactivation. *Nature.* 2010;468(7326):968-72
53. Christoforidou AV, Papadaki HA, Margioris AN, Eliopoulos GD, and Tsatsanis C. Expression of the Tpl2/Cot oncogene in human T-cell neoplasias. *Mol Cancer.* 2004;3(1):34
54. Clark AM, Reynolds SH, Anderson M, and Wiest JS. Mutational activation of the MAP3K8 protooncogene in lung cancer. *Genes Chromosomes Cancer.* 2004;41(2):99-108
55. Sourvinos G, Tsatsanis C, and Spandidos DA. Overexpression of the Tpl-2/Cot oncogene in human breast cancer. *Oncogene.* 1999;18(35):4968-73
56. von Bernuth H, Picard C, Puel A, and Casanova JL. Experimental and natural infections in MyD88- and IRAK-4-deficient mice and humans. *Eur J Immunol.* 2012;42(12):3126-35
57. Rosenthal AC, Tun HW, Younes A, Nowakowski GS, Lunning MA, Patel K, Landsburg DJ, Martell RE, and Leslie LA. Phase 1 study of CA-4948, a novel inhibitor of interleukin-1 receptor-associated kinase 4 (IRAK4) in patients (pts) with r/r non-Hodgkin lymphoma. *Journal of Clinical Oncology.* 2019;37(15_suppl):e19055-e
58. Dumitru CD, Ceci JD, Tsatsanis C, Kontoyiannis D, Stamatakis K, Lin JH, Patriotis C, Jenkins NA, Copeland NG, Kollias G, et al. TNF-alpha induction by LPS is regulated posttranscriptionally via a Tpl2/ERK-dependent pathway. *Cell.* 2000;103(7):1071-83
59. Shoemaker RH. The NCI60 human tumour cell line anticancer drug screen. *Nat Rev Cancer.* 2006;6(10):813-23

60. Lim KH, Baines AT, Fiordalisi JJ, Shipitsin M, Feig LA, Cox AD, Der CJ, and Counter CM. Activation of RalA is critical for Ras-induced tumorigenesis of human cells. *Cancer Cell.* 2005;7(6):533-45
61. Jiang H, Hegde S, Knolhoff BL, Zhu Y, Herndon JM, Meyer MA, Nywening TM, Hawkins WG, Shapiro IM, Weaver DT, et al. Targeting focal adhesion kinase renders pancreatic cancers responsive to checkpoint immunotherapy. *Nat Med.* 2016;22(8):851-60
62. Durkin ME, Qian X, Popescu NC, and Lowy DR. Isolation of Mouse Embryo Fibroblasts. *Bio Protoc.* 2013;3(18)
63. Jones S, Zhang X, Parsons DW, Lin JC, Leary RJ, Angenendt P, Mankoo P, Carter H, Kamiyama H, Jimeno A, et al. Core signaling pathways in human pancreatic cancers revealed by global genomic analyses. *Science.* 2008;321(5897):1801-6
64. Kim MP, Evans DB, Wang H, Abbruzzese JL, Fleming JB, and Gallick GE. Generation of orthotopic and heterotopic human pancreatic cancer xenografts in immunodeficient mice. *Nat Protoc.* 2009;4(11):1670-80
65. Lim KH, Langley E, Gao F, Luo J, Li L, Meyer G, Kim P, Singh S, Kushnir VM, Early DS, et al. A clinically feasible multiplex proteomic immunoassay as a novel functional diagnostic for pancreatic ductal adenocarcinoma. *Oncotarget.* 2017;8(15):24250-61

Figure Legends and Figures

Figure 1. IRAK signaling dictates NF-κB activity in PDAC and is essential for RAS-oncogenesis

(A) Classification of *RELA* low, medium and high patients based on mRNA z-score from TCGA. **(B)** Progression free survival (PFS) and overall survival (OS) of PDAC patients with high versus low *RELA* expression. **(C)** Heatmap comparing mRNA expression of NF-κB signature genes from the Broad Institute Molecular Signatures Database (gene-sets are listed in **Supplementary Table 3**) in $RELA^{high}$ vs. $RELA^{low}$ patients. **(D** and **E)** PFS and disease-free status respectively of PDAC patients with high *MYD88* and/or high *IRAK1* expression ("$MYD88^{High}$, $IRAK1^{High}$") versus low *MYD88* and/or low *IRAK1* expression ("$MYD88^{Low}$, $IRAK1^{Low}$"). Eight patients overlapping between two groups were excluded. **(F** and **G)** OS and vital status of patients as in **(D** and **E). (H)** Graph of *IRAK4* expression in normal human pancreas versus PDAC. Data for normal tissue is from The Genotype-Tissue Expression (GTEx) project and PDAC expression from TCGA PanCancer Atlas. *P*-values are from unpaired two-sided *t*-test. **(I)** Soft agar colonies formed by *Irak4*-KO and rescue (KO + $Irak4^{WT}$) MEF cells transformed with three pairs of oncogenes. Data shows nine replicates from three independent experiments. **(J)** Number of tumors formed in nude mice from subcutaneous implantation of WT and *IRAK4*-KO human and murine *RAS*-mutant and/or PDAC cell lines. $n = 8$ tumors per condition. **(K)** Quantification of soft agar colonies formed by WT versus *Irak4*-KO KP2 cells. Data shows six replicates from two independent experiments. **(L)** Soft agar colonies formed by KP2 cells treated with IRAK4i. **(M)** Soft agar colonies formed by WT and $KRAS^{G12D}$ HPNE cells ectopically expressing *IRAK4* WT and treated with IRAK4i. For **(L)** and **(M)** three independent experiments were performed, each in technical triplicate, and one set of data is shown. All error bars indicate mean ± SEM; ****$P<0.0001$, ***$P<0.0002$, **$P<0.0021$, *$P<0.0332$.

Figure 1

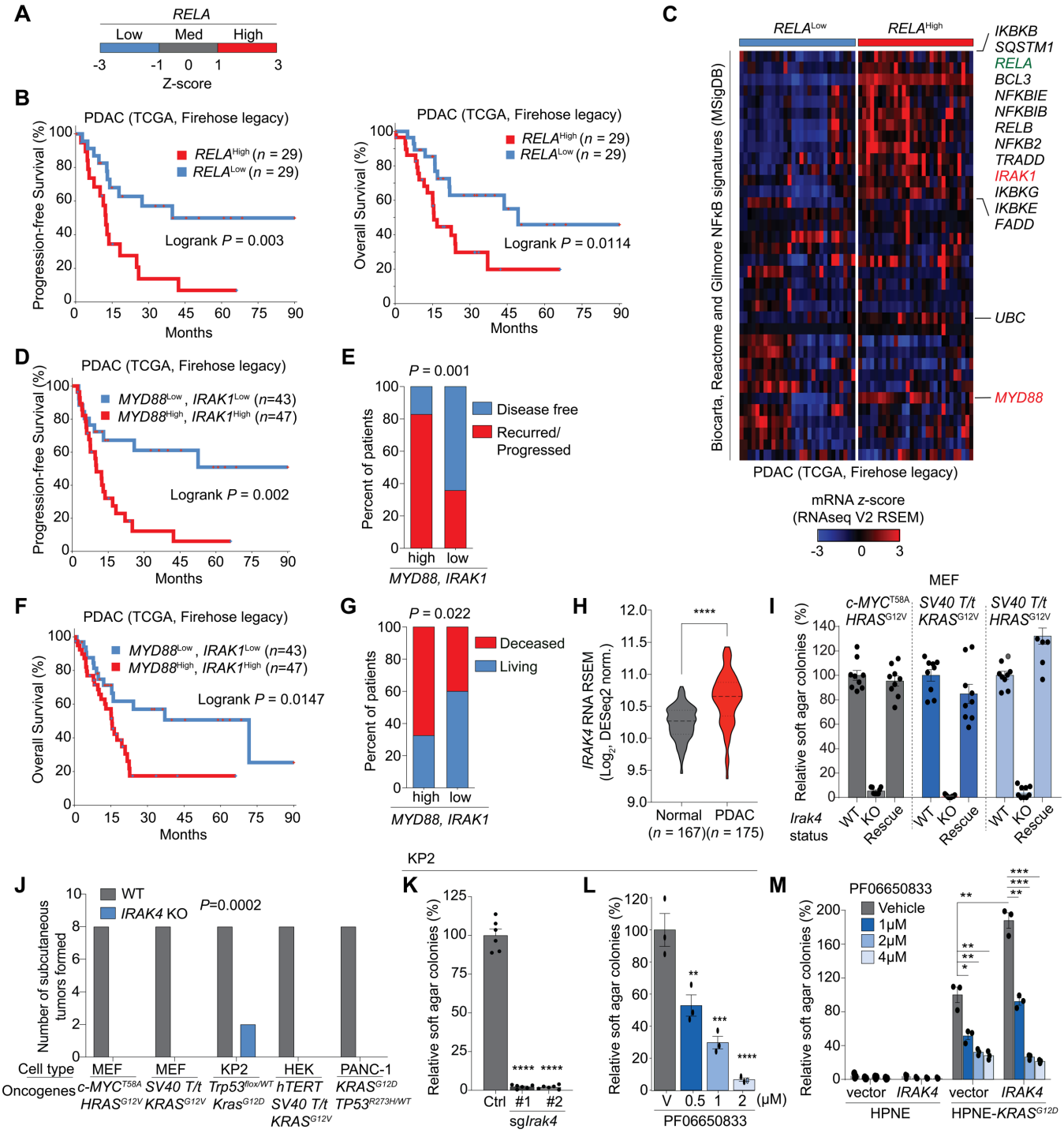
A
RELA
Low
Med
High
-3
-1
0
1
3
Z-score
B
PDAC (TCGA, Firehose legacy)
Progression-free Survival (%)
RELA^High (n = 29)
RELA^Low (n = 29)
Logrank P = 0.003
Months
PDAC (TCGA, Firehose legacy)
Overall Survival (%)
RELA^High (n = 29)
RELA^Low (n = 29)
Logrank P = 0.0114
Months
C
RELA^Low
RELA^High
IKBKB
SQSTM1
RELA
BCL3
NFKBIE
NFKBIB
RELB
NFKB2
TRADD
IRAK1
IKBKG
IKBKE
FADD
UBC
MYD88
Biocarta, Reactome and Gilmore NFκB signatures (MSigDB)
PDAC (TCGA, Firehose legacy)
mRNA z-score
(RNAseq V2 RSEM)
-3
0
3
D
PDAC (TCGA, Firehose legacy)
Progression-free Survival (%)
MYD88^Low, IRAK1^Low (n=43)
MYD88^High, IRAK1^High (n=47)
Logrank P = 0.002
Months
E
P = 0.001
Percent of patients
Disease free
Recurred/
Progressed
high
low
MYD88, IRAK1
F
PDAC (TCGA, Firehose legacy)
Overall Survival (%)
MYD88^Low, IRAK1^Low (n=43)
MYD88^High, IRAK1^High (n=47)
Logrank P = 0.0147
Months
G
P = 0.022
Percent of patients
Deceased
Living
high
low
MYD88, IRAK1
H
****
IRAK4 RNA RSEM
(Log2, DESeq2 norm.)
Normal
(n = 167)
PDAC
(n = 175)
I
MEF
c-MYC^T58A
HRAS^G12V
SV40 T/t
KRAS^G12V
SV40 T/t
HRAS^G12V
Relative soft agar colonies (%)
Irak4
status
WT
KO
Rescue
J
WT
IRAK4 KO
P=0.0002
Number of subcutaneous
tumors formed
Cell type
Oncogenes
MEF
c-MYC^T58A
HRAS^G12V
MEF
SV40 T/t
KRAS^G12V
KP2
Trp53^flox/WT
Kras^G12D
HEK
hTERT
SV40 T/t
KRAS^G12V
PANC-1
KRAS^G12D
TP53^R273H/WT
KP2
K
Relative soft agar colonies (%)
****
****
Ctrl
#1
#2
sgIrak4
L
Relative soft agar colonies (%)
**
***
****
V
0.5
1
2
(μM)
PF06650833
M
PF06650833
Vehicle
1μM
2μM
4μM
Relative soft agar colonies (%)
vector
IRAK4
HPNE
vector
IRAK4
HPNE-KRAS^G12D

Figure 2. IRAK4 is crucial for oncogenic RAS-driven MAPK signaling

(A) Linear fold-change for all targets evaluated by reverse-phase protein array performed on HPNE-*KRAS*^{G12D} overexpressing *IRAK4* and treated with IRAK4i. Targets with fold change >2 upon IRAK4 overexpression are identified. **(B)** Heat map showing relative expression of ERK regulated targets in RPPA shown in **(A). (C)** Immunoblots of 293T cells transfected with AU1 epitope-tagged WT or kinase-dead *IRAK4*. **(D)** Heat-map depicting fold-change for MAPK, RAS and cell growth related Gene Ontology (GO) signatures upon *Irak4* knock-out (KO) and rescue (KO + *Irak4*^{WT}) in murine KP2 cells. Comparisons are KO vs. WT and Rescue vs. KO. Signatures significantly ($P < 0.05$) depleted (blue) or enriched (red) are marked with an asterisk (*). **(E)** Immunoblots of WT and *Irak4*-KO KP2 cells. **(F** and **G)** Gene set enrichment plot and normalized enrichment scores respectively for signatures associated with oncogenic *KRAS* in WT, *Irak4*-KO, and rescue KP2 cells, compared as in **(D)**. "Hallmark" and "C6: Oncogenic Signatures" databases were utilized. Negative NES indicates downregulation and signatures significantly ($P < 0.05$) depleted (blue) or enriched (red) are marked with an asterisk (*). **(H)** Gene set enrichment plot for PDAC signature in *Irak4*-KO and rescue KP2 cells. PDAC signature gene list is provided in **Supplementary Table 3**. **(I)** Immunoblots of KP2 and KI cells treated with IRAK4i (PF06650833) for 24 hours in serum-free condition. **(J)** Immunoblots of PDAC cells treated with IRAK4i for 16 hours. **(K)** Immunoblots of HPNE-*KRAS*^{G12D} and 293T-*KRAS*^{G12V} cells treated with IRAK4i for 24hrs in serum-free media. For **(D** and **F**-**H)** RNAseq was performed as $n = 2$ independent samples for each condition.

Figure 2

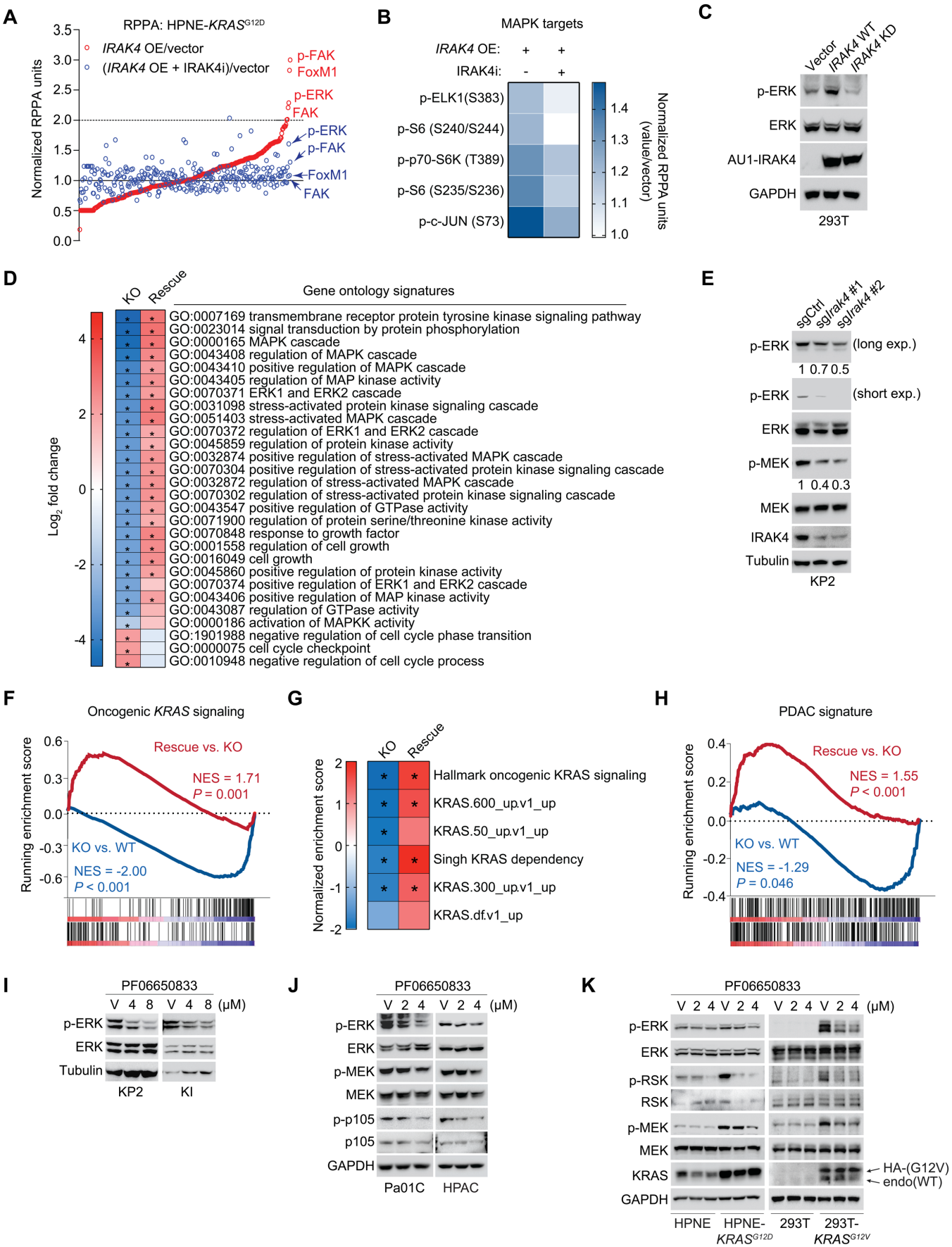
A
RPPA: HPNE-KRASG12D
IRAK4 OE/vector
(IRAK4 OE + IRAK4i)/vector
Normalized RPPA units
p-FAK
FoxM1
p-ERK
FAK
p-ERK
p-FAK
FoxM1
FAK
B
MAPK targets
IRAK4 OE:
IRAK4i:
p-ELK1(S383)
p-S6 (S240/S244)
p-p70-S6K (T389)
p-S6 (S235/S236)
p-c-JUN (S73)
Normalized RPPA units (value/vector)
C
Vector
IRAK4 WT
IRAK4 KD
p-ERK
ERK
AU1-IRAK4
GAPDH
293T
D
KO
Rescue
Gene ontology signatures
Log2 fold change
GO:0007169 transmembrane receptor protein tyrosine kinase signaling pathway
GO:0023014 signal transduction by protein phosphorylation
GO:0000165 MAPK cascade
GO:0043408 regulation of MAPK cascade
GO:0043410 positive regulation of MAPK cascade
GO:0043405 regulation of MAP kinase activity
GO:0070371 ERK1 and ERK2 cascade
GO:0031098 stress-activated protein kinase signaling cascade
GO:0051403 stress-activated MAPK cascade
GO:0070372 regulation of ERK1 and ERK2 cascade
GO:0045859 regulation of protein kinase activity
GO:0032874 positive regulation of stress-activated MAPK cascade
GO:0070304 positive regulation of stress-activated protein kinase signaling cascade
GO:0032872 regulation of stress-activated MAPK cascade
GO:0070302 regulation of stress-activated protein kinase signaling cascade
GO:0043547 positive regulation of GTPase activity
GO:0071900 regulation of protein serine/threonine kinase activity
GO:0070848 response to growth factor
GO:0001558 regulation of cell growth
GO:0016049 cell growth
GO:0045860 positive regulation of protein kinase activity
GO:0070374 positive regulation of ERK1 and ERK2 cascade
GO:0043406 positive regulation of MAP kinase activity
GO:0043087 regulation of GTPase activity
GO:0000186 activation of MAPKK activity
GO:1901988 negative regulation of cell cycle phase transition
GO:0000075 cell cycle checkpoint
GO:0010948 negative regulation of cell cycle process
E
sgCtrl
sgIrak4 #1
sgIrak4 #2
p-ERK
(long exp.)
1 0.7 0.5
p-ERK
(short exp.)
ERK
p-MEK
1 0.4 0.3
MEK
IRAK4
Tubulin
KP2
F
Oncogenic KRAS signaling
Running enrichment score
Rescue vs. KO
NES = 1.71
P = 0.001
KO vs. WT
NES = -2.00
P < 0.001
G
KO
Rescue
Normalized enrichment score
Hallmark oncogenic KRAS signaling
KRAS.600_up.v1_up
KRAS.50_up.v1_up
Singh KRAS dependency
KRAS.300_up.v1_up
KRAS.df.v1_up
H
PDAC signature
Running enrichment score
Rescue vs. KO
NES = 1.55
P < 0.001
KO vs. WT
NES = -1.29
P = 0.046
I
PF06650833
V 4 8 V 4 8 (μM)
p-ERK
ERK
Tubulin
KP2
KI
J
PF06650833
V 2 4 V 2 4 (μM)
p-ERK
ERK
p-MEK
MEK
p-p105
p105
GAPDH
Pa01C
HPAC
K
PF06650833
V 2 4 V 2 4 V 2 4 V 2 4 (μM)
p-ERK
ERK
p-RSK
RSK
p-MEK
MEK
KRAS
GAPDH
HA-(G12V)
endo(WT)
HPNE
HPNE-KRASG12D
293T
293T-KRASG12V

Figure 3. TPL2 mediates signaling between IRAK4 and MAPK pathway

(A) Immunoblot of Pa01C cells overexpressing HA epitope-tagged TPL2 WT that were treated with IRAK4i for 6 hours in serum-free condition. **(B)** Immunoblots of 293T cells transfected with *IRAK4* WT for 48 hours. **(B)** Leading-edge analysis performed using data generated by gene set enrichment analysis in order to identify alterations in individual genes within each gene-set tested. Significantly down-regulated ($P < 0.05$) gene signatures were analyzed and clustered heat-map was generated. Section of heat-map depicting change in *MAP3K8* (TPL2) and *MAP2K1* (MEK1) expression is shown with original clustering preserved. TPL2 associated gene set list is provided in **Supplementary Table 3. (D)** Immunoblot of various commercially available and patient-derived (Pa01C-Pa16C) human PDAC cell lines and one normal human pancreatic cell line (HPNE). **(E)** Correlation plot of p-ERK and TPL2 intensities for PDAC cell lines in **(D).** Two-tailed Pearson correlation (*r)* analysis was performed. **(F)** Representative H&E and immunohistochemistry images of human and murine normal pancreas and PDAC tissue for p-ERK, TPL2 and p-IRAK4. $n = 6$ sections per stain. Scale bar for full image (400X magnification) measures 50μm; inset shows magnified boxed portion of full images with scale bar measuring 10μm.

925 **Figure 3**

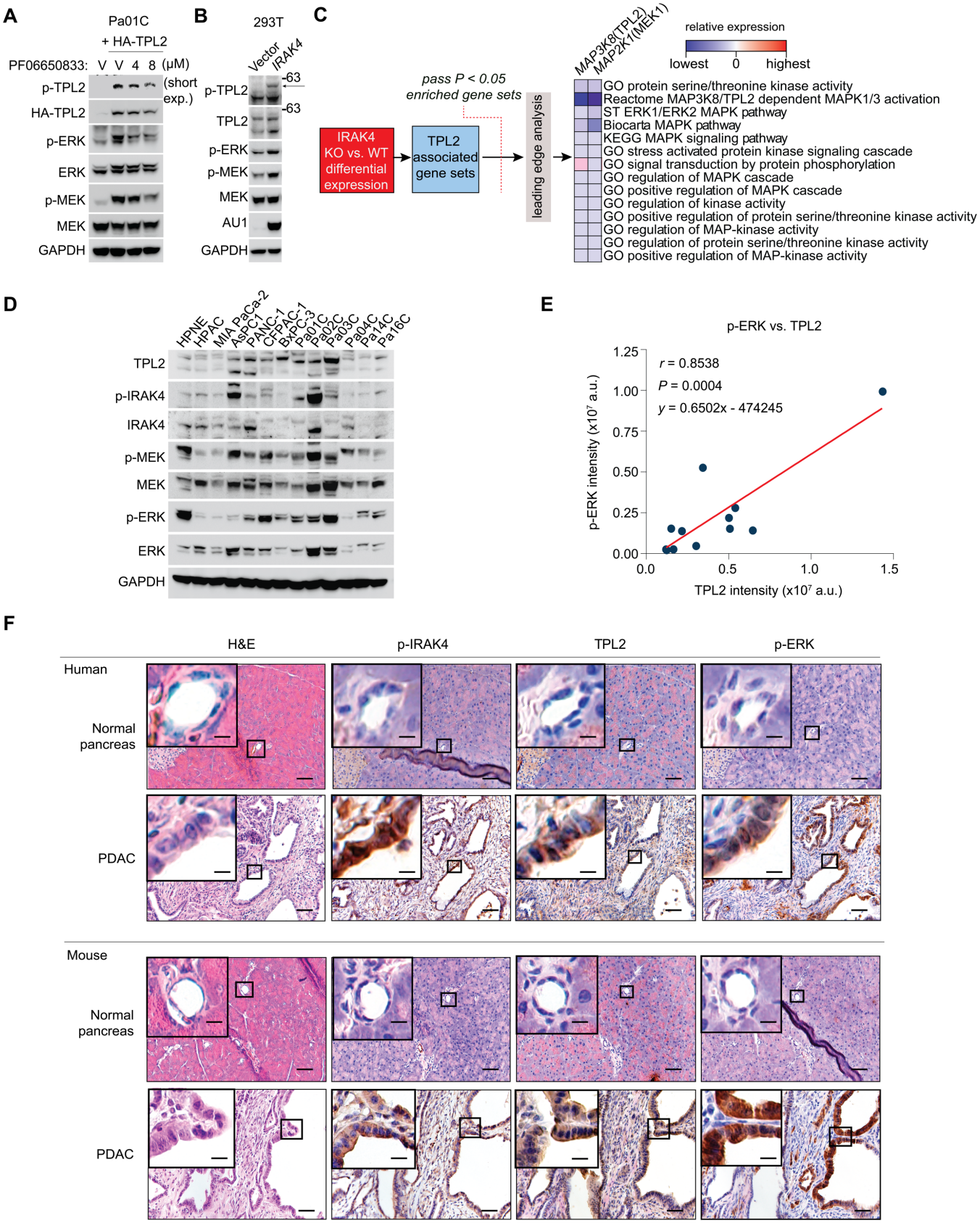
A
Pa01C
+ HA-TPL2
PF06650833: V V 4 8 (μM)
p-TPL2
(short exp.)
HA-TPL2
p-ERK
ERK
p-MEK
MEK
GAPDH
B
293T
Vector
IRAK4
p-TPL2
TPL2
p-ERK
p-MEK
MEK
AU1
GAPDH
63
63
C
IRAK4 KO vs. WT differential expression
TPL2 associated gene sets
pass P < 0.05 enriched gene sets
leading edge analysis
MAP3K8(TPL2)
MAP2K1(MEK1)
relative expression
lowest 0 highest
GO protein serine/threonine kinase activity
Reactome MAP3K8/TPL2 dependent MAPK1/3 activation
ST ERK1/ERK2 MAPK pathway
Biocarta MAPK pathway
KEGG MAPK signaling pathway
GO stress activated protein kinase signaling cascade
GO signal transduction by protein phosphorylation
GO regulation of MAPK cascade
GO positive regulation of MAPK cascade
GO regulation of kinase activity
GO positive regulation of protein serine/threonine kinase activity
GO regulation of MAP-kinase activity
GO regulation of protein serine/threonine kinase activity
GO positive regulation of MAP-kinase activity
D
HPNE
HPAC
MIA PaCa-2
AsPC1
PANC-1
CFPAC-1
BxPC-3
Pa01C
Pa02C
Pa03C
Pa04C
Pa14C
Pa16C
TPL2
p-IRAK4
IRAK4
p-MEK
MEK
p-ERK
ERK
GAPDH
E
p-ERK vs. TPL2
r = 0.8538
P = 0.0004
y = 0.6502x - 474245
p-ERK intensity (x10^7 a.u.)
TPL2 intensity (x10^7 a.u.)
1.25
1.00
0.75
0.50
0.25
0.00
0.0
0.5
1.0
1.5
F
H&E
p-IRAK4
TPL2
p-ERK
Human
Normal pancreas
PDAC
Mouse
Normal pancreas
PDAC

Figure 4. High TPL2 expression is poor prognostic in PDAC

(A) IHC images representing high and low staining H-scores for TPL2 and p-IRAK4 with and without HALO analysis markup. H score = 3*(% of strongly stained area) + 2*(% of strongly stained area) + 1*(% of weakly stained area). **(B)** Spearman (*r*) correlation plot of TPL2 and p-IRAK4 H-scores from tissue-micro-array (TMA) analysis of 313 tissue specimens from 157 PDAC patients, represented in **(A). (C)** Kaplan-Meier comparing survival of patients with high vs. low TPL2 protein expression based on analysis of TMA above. **(D)** Graph depicting *MAP3K8* (TPL2) expression in normal human pancreas versus PDAC tissue. Data for normal pancreas tissue is from The Genotype-Tissue Expression (GTEx) project and PDAC expression was from the pancreatic adenocarcinoma TCGA PanCancer Atlas study. *P*-values are from unpaired two-sided *t*-test. Outliers (5 in normal, 3 in PDAC) were removed by ROUT, Q = 0.1%. **(E)** Graph of overall survival (OS) of TCGA PDAC patients separated into short and longer survivor cohorts using median OS of ~15.5 months. **(F)** Graph comparing *MAP3K8* mRNA expression in longer vs. short survivors defined in **(E).** *P*-values are from unpaired, two-sided *t*-test. All 178 (out of 185) TCGA PDAC samples with mRNA expression data were analyzed. **(G)** Graph comparing months of overall survival of patients with high (z score > 1, $n = 22$) versus low (z score < 1, $n = 28$) *MAP3K8* expression based on analysis of TCGA Firehose Legacy dataset. *P* values from Kruskal Wallis test. ****$P<0.0001$, ***$P<0.0002$, **$P<0.0021$, *$P<0.0332$.

Figure 4

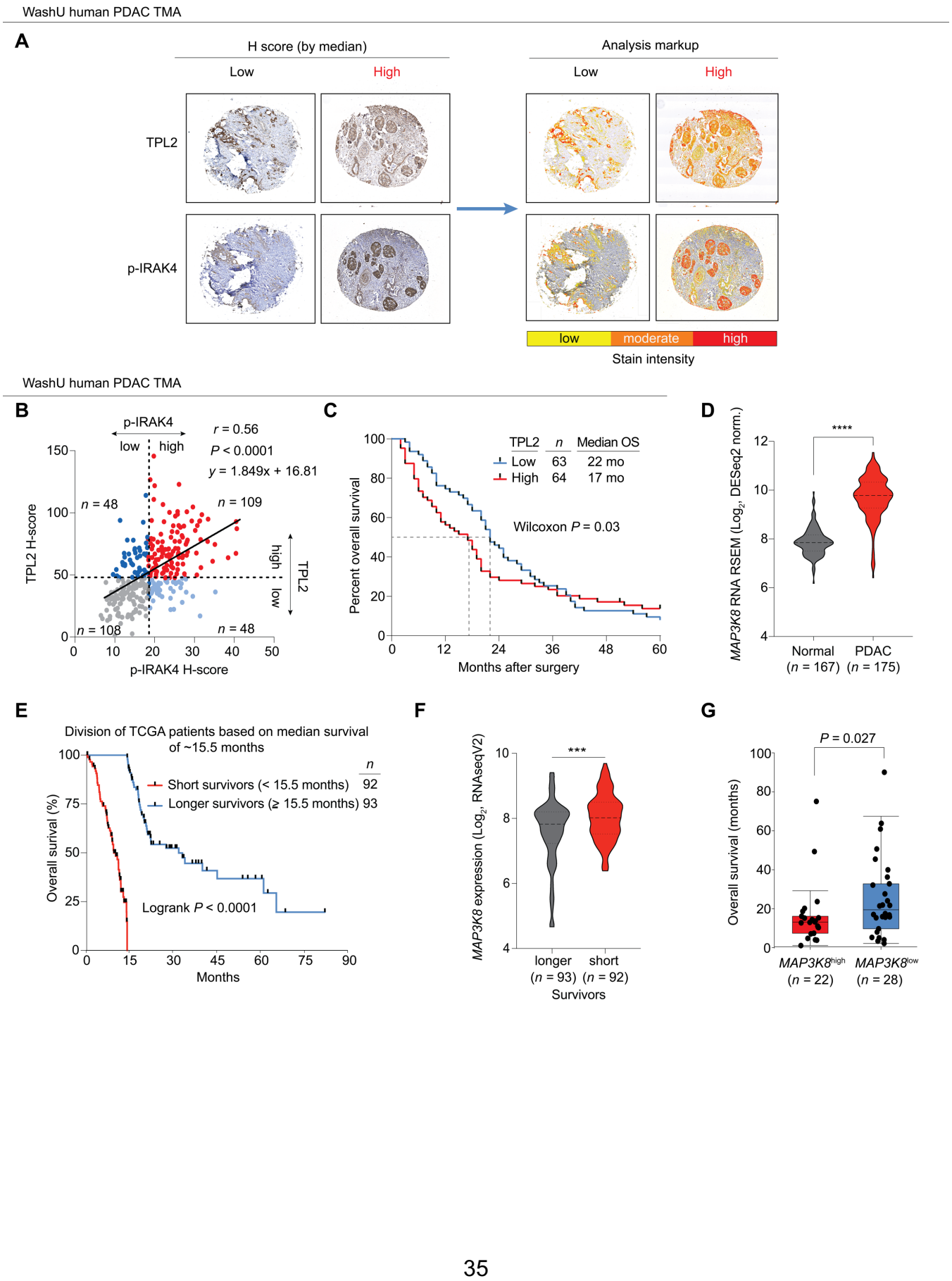
WashU human PDAC TMA
A
H score (by median)
Low
High
Analysis markup
Low
High
TPL2
p-IRAK4
low
moderate
high
Stain intensity
WashU human PDAC TMA
B
p-IRAK4
low
high
r = 0.56
P < 0.0001
y = 1.849x + 16.81
n = 48
n = 109
n = 108
n = 48
TPL2 H-score
p-IRAK4 H-score
high
low
TPL2
C
TPL2 n Median OS
Low 63 22 mo
High 64 17 mo
Wilcoxon P = 0.03
Percent overall survival
Months after surgery
D
MAP3K8 RNA RSEM (Log2, DESeq2 norm.)
****
Normal (n = 167)
PDAC (n = 175)
E
Division of TCGA patients based on median survival of ~15.5 months
n
Short survivors (< 15.5 months) 92
Longer survivors (≥ 15.5 months) 93
Logrank P < 0.0001
Overall surival (%)
Months
F
MAP3K8 expression (Log2, RNAseqV2)
***
longer (n = 93)
short (n = 92)
Survivors
G
P = 0.027
Overall survival (months)
MAP3K8high (n = 22)
MAP3K8low (n = 28)

Figure 5. TPL2 drives both MAPK and NFκB signaling in PDAC

(A) Gene set enrichment plots for patients with high (z score > 1, *n* = 22) and low (z score < 1, *n* = 28) *MAP3K8* expression from TCGA Firehose legacy study. **(B)** Immunoblots of *KRAS* mutant human PDAC cell lines treated with TPL2 inhibitor (TPL2i) for 36 hours in serum-free media. **(C)** Immunoblots of 293T and 293T-*KRAS*^{G12V} cells treated with TPL2i for 24 hours in serum-free condition. **(D)** Immunoblots of Pa01C cells treated with incremental doses of TPL2i. **(E)** Immunoblots of PDAC cell lines treated with TPL2i. **(F)** Serum-response element (SRE) reporter assay of HPAC cells treated with TPL2i, BRAFi, MEKi or ERKi. Data shows three independent experiments each done in triplicate. **(G)** Quantification of soft agar colonies formed by PDAC cell lines treated with TPL2i. Data represents *n* = 3 (*n* = 2 for CFPAC-1) for each cell line. One data point shown per biological replicate, each consisting of three technical replicates. *P* values from two-way ANOVA with Dunnett's multiple comparison test. **(H)** Immunoblots of WT or *MAP3K8* (TPL2) knockdown HPAC cells. **(I)** Quantification of HPAC and Pa01C cell proliferation after TPL2 knockdown with shRNA (sh*MAP3K8*). Each data point is average of six replicates. *P* values by two-way ANOVA with Dunnett's multiple comparison test. **(J)** Representative crystal violet stained images of 2D colony formation of TPL2 knockdown HPAC and Pa01C cells. **(K)** Light microscopic images of organoids formed by HPAC and Pa01C cells with TPL2 knockdown. Scale bar is 100μm for full image, and 25μm for magnified inset. Graph on right is quantification of number of organoids formed in three independent wells. *P* values by two-way ANOVA with Dunnett's multiple comparison test. All error bars indicate mean ± SEM; ****P<0.0001, ***P<0.0002, **P<0.0021, *P<0.0332.

Figure 5

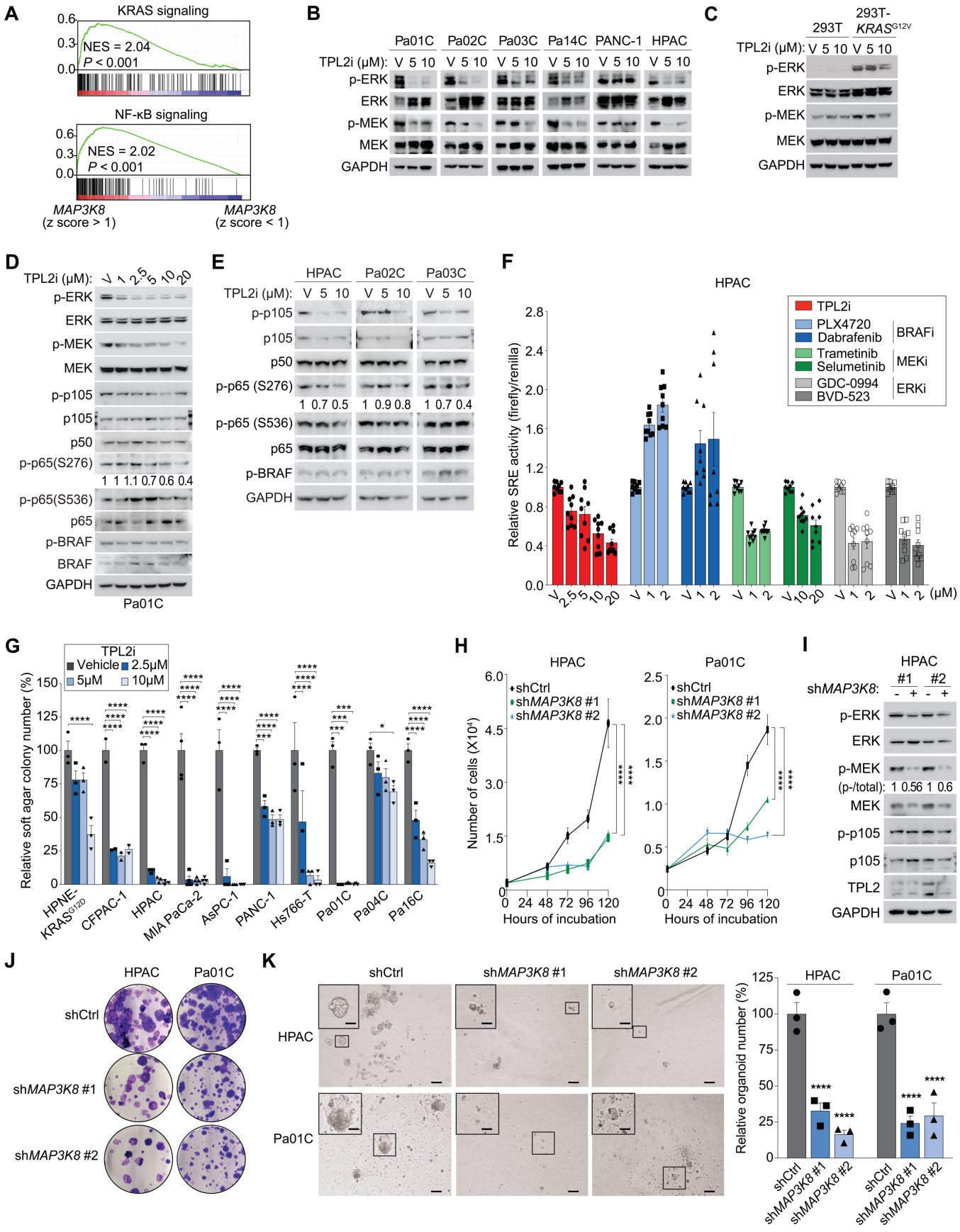
A
KRAS signaling
NES = 2.04
P < 0.001
NF-κB signaling
NES = 2.02
P < 0.001
MAP3K8 (z score > 1)
MAP3K8 (z score < 1)
B
Pa01C Pa02C Pa03C Pa14C PANC-1 HPAC
TPL2i (μM): V 5 10 V 5 10 V 5 10 V 5 10 V 5 10 V 5 10
p-ERK
ERK
p-MEK
MEK
GAPDH
C
293T
293T-KRASG12V
TPL2i (μM): V 5 10 V 5 10
p-ERK
ERK
p-MEK
MEK
GAPDH
D
TPL2i (μM): V 1 2.5 5 10 20
p-ERK
ERK
p-MEK
MEK
p-p105
p105
p50
p-p65(S276)
1 1 1.1 0.7 0.6 0.4
p-p65(S536)
p65
p-BRAF
BRAF
GAPDH
Pa01C
E
HPAC Pa02C Pa03C
TPL2i (μM): V 5 10 V 5 10 V 5 10
p-p105
p105
p50
p-p65 (S276)
1 0.7 0.5 1 0.9 0.8 1 0.7 0.4
p-p65 (S536)
p65
p-BRAF
GAPDH
F
HPAC
TPL2i
PLX4720
Dabrafenib
BRAFi
Trametinib
Selumetinib
MEKi
GDC-0994
BVD-523
ERKi
Relative SRE activity (firefly/renilla)
(μM)
G
TPL2i
Vehicle 2.5μM
5μM 10μM
Relative soft agar colony number (%)
HPNE-KRASG12D
CFPAC-1
HPAC
MIA PaCa-2
AsPC-1
PANC-1
Hs766-T
Pa01C
Pa04C
Pa16C
H
HPAC
Pa01C
shCtrl
shMAP3K8 #1
shMAP3K8 #2
Number of cells (X10⁴)
Hours of incubation
I
HPAC
shMAP3K8: #1 #2
p-ERK
ERK
p-MEK
(p-/total): 1 0.56 1 0.6
MEK
p-p105
p105
TPL2
GAPDH
J
HPAC Pa01C
shCtrl
shMAP3K8 #1
shMAP3K8 #2
K
shCtrl
shMAP3K8 #1
shMAP3K8 #2
HPAC
Pa01C
Relative organoid number (%)

Figure 6. KRAS induces autocrine IL-1β signaling activates IRAK4 and TPL2

(A) qRT-PCR of HEK cells expressing empty vector or *KRAS*^{G12V}. Data shows six replicates from two independent experiments. *P* values from two-way ANOVA with Dunnett's multiple-comparison test. **(B)** Heatmap of Hallmark "KRAS signaling up" signature in *MAP3K8* high vs. low patients. *IL1B* is significantly enriched in *MAP3K8*^{high} patients, shown also in box-plot on right. **(C)** Immunoblots of HEK-*KRAS*^{G12V} cells treated with anti-hIL-1β neutralizing antibody for 24 hours. **(D)** Immunoblots of HEK cells incubated with conditioned media (CM) from HEK-*KRAS*^{G12V} cells (called "*KRAS*^{G12V} CM") and anti-hIL-1β neutralizing antibody. **(E)** Immunoblots of HEK cells incubated with *KRAS*^{G12V} CM and TPL2i for 16 hours. **(F)** Immunoblots of HEK and HPAC cells overexpressing HA epitope-tagged TPL2 WT stimulated with 100ng mL^{-1} recombinant hIL-1β for indicated duration. **(G)** Immunoblots of HEK cells expressing *KRAS*^{G12V}, HA epitope tagged TPL2 WT and sh*IL1R1*. **(H)** Kaplan-Meier curve of PDAC TCGA patients with high vs. low *IL1B* expression. Follow-up censored at 60 months. All error bars indicate mean ± SEM; ****P<0.0001, ***P<0.0002, **P<0.0021, *P<0.0332.

1045 **Figure 6**

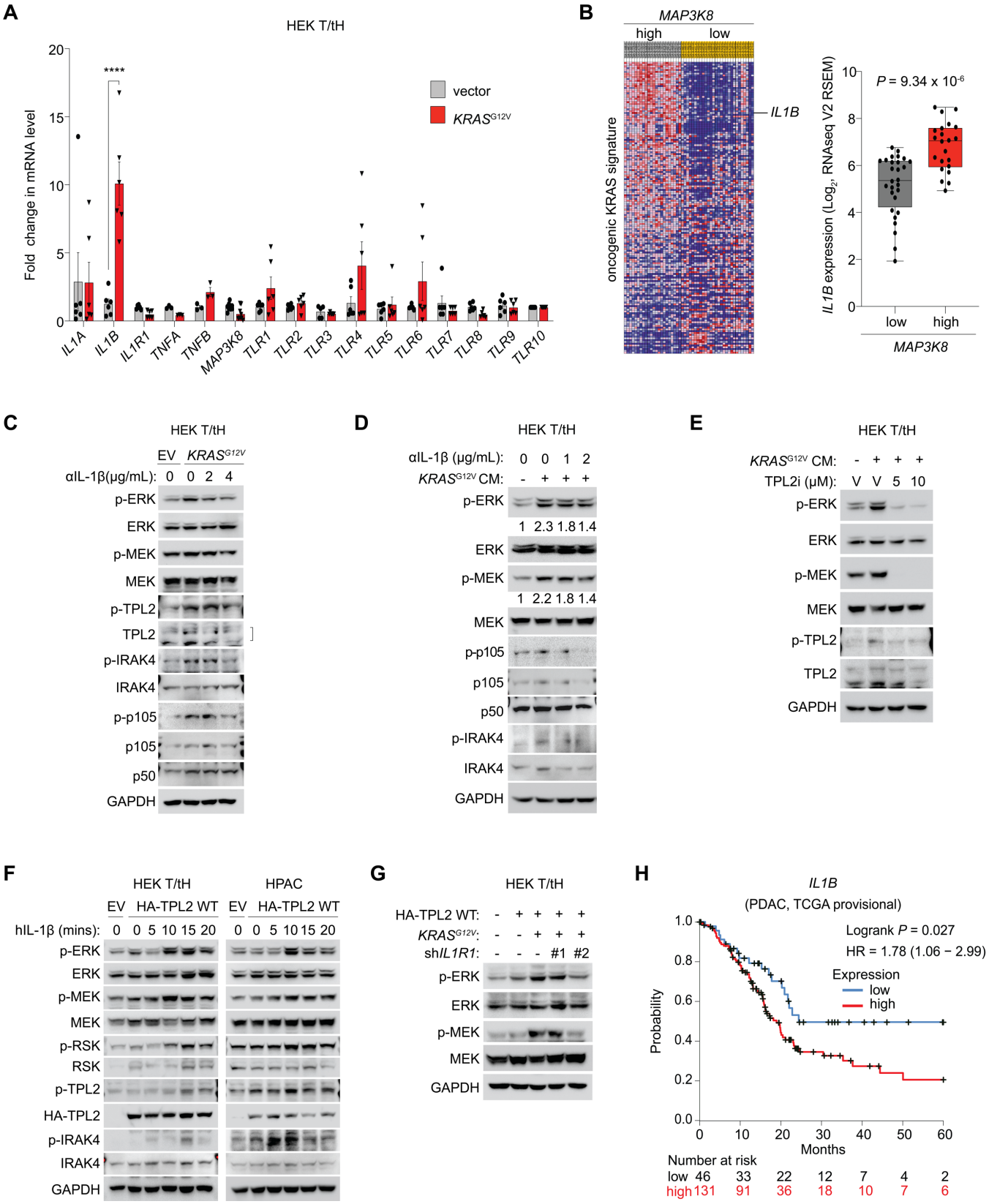

Figure 7. TPL2 inhibition potentiates chemotherapy by curbing MAPK and NF-κB activation

(A) Immunoblots of two PDAC cell lines overexpressing HA epitope-tagged TPL2 WT treated for 16 hours with different chemotherapy agents (10μM each). **(B-C)** Quantification of mRNA transcript levels for multiple genes in three PDAC cell lines treated with vehicle, gemcitabine-paclitaxel (Gem-PTX) or FIRINOX (10μM each of 5-FU, SN-38 and oxaliplatin). **(D)** Duolink® proximity ligase assay identifying interaction of p-IRAK4 and TLR9 in three PDAC cell lines treated with 10μM SN-38 for 16 hours. Six 400X magnification fields per condition were analyzed. Scale bars represent 10μm. **(E)** Immunoblots of three PDAC cell lines treated with TPL2i, SN-38 or the combination for 16 hours. **(F)** 2D crystal violet clonogenic colony forming assays of three PDAC cell lines treated with TPL2i, SN-38 (2.5nM, 5nM and 10nM) or the combination in a dose matrix for three to four weeks. Data shows one independent experiment out of ≥3 per cell line **(G)** Tumor volume curves for patient derived Pa01C PDAC cells implanted subcutaneously into nude mice followed by treatment with TPL2 inhibitor, FIRINOX, or combination therapy. Data represents 10 independent tumors (n = 10) for each drug treatment group and 8 independent tumors (n = 8) for vehicle treated group. P value from two-way ANOVA followed by Tukey's multiple comparison test. One outlier was removed by Grubb's, alpha = 0.01. **(H)** Graph depicting final tumor weight (final pancreas weight – 0.1g (i.e. normal pancreas weight)) after orthoptic injection of murine KI cells and treatment as indicated for 14 days. Images of ex vivo and in vivo tumors detected by ultrasound along with tumor volume are shown on right. P values from one-way ANOVA with Tukey's multiple comparison test. All error bars indicate mean ± SEM; ****P<0.0001, ***P<0.0002, **P<0.0021, *P<0.0332.

Figure 7

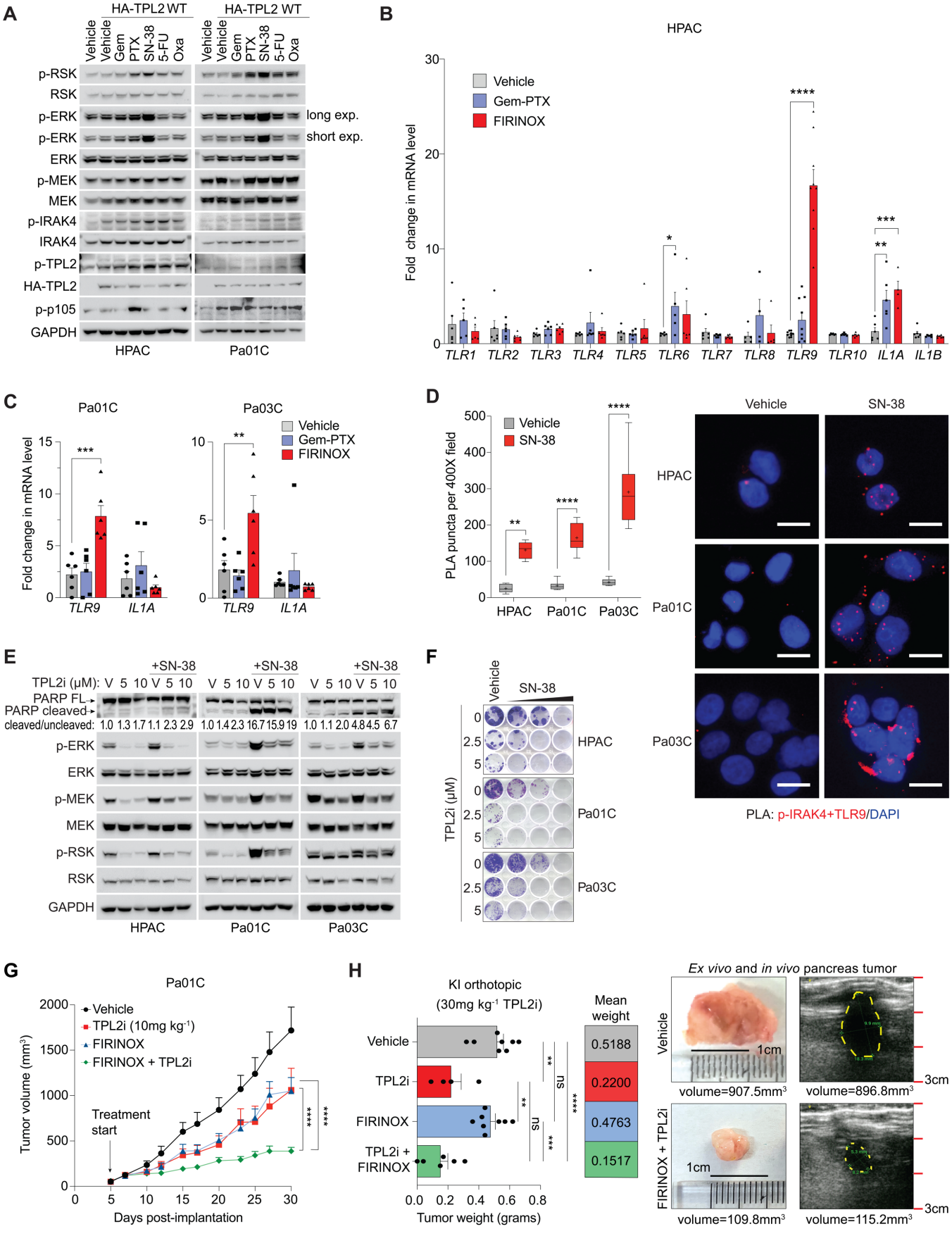
A
HA-TPL2 WT
HA-TPL2 WT
Vehicle
Vehicle
Gem
PTX
SN-38
5-FU
Oxa
p-RSK
RSK
p-ERK
p-ERK
long exp.
short exp.
ERK
p-MEK
MEK
p-IRAK4
IRAK4
p-TPL2
HA-TPL2
p-p105
GAPDH
HPAC
Pa01C
B
HPAC
Vehicle
Gem-PTX
FIRINOX
Fold change in mRNA level
TLR1
TLR2
TLR3
TLR4
TLR5
TLR6
TLR7
TLR8
TLR9
TLR10
IL1A
IL1B
C
Pa01C
Pa03C
Vehicle
Gem-PTX
FIRINOX
Fold change in mRNA level
TLR9
IL1A
D
Vehicle
SN-38
PLA puncta per 400X field
HPAC
Pa01C
Pa03C
Vehicle
SN-38
HPAC
Pa01C
Pa03C
PLA: p-IRAK4+TLR9/DAPI
E
+SN-38
TPL2i (μM): V 5 10 V 5 10
PARP FL
PARP cleaved
cleaved/uncleaved: 1.0 1.3 1.7 1.1 2.3 2.9 1.0 1.4 2.3 16.7 15.9 19 1.0 1.1 2.0 4.8 4.5 6.7
p-ERK
ERK
p-MEK
MEK
p-RSK
RSK
GAPDH
HPAC
Pa01C
Pa03C
F
Vehicle
SN-38
TPL2i (μM)
HPAC
Pa01C
Pa03C
G
Pa01C
Vehicle
TPL2i (10mg kg-1)
FIRINOX
FIRINOX + TPL2i
Tumor volume (mm3)
Treatment start
Days post-implantation
H
KI orthotopic
(30mg kg-1 TPL2i)
Mean weight
Vehicle
TPL2i
FIRINOX
TPL2i + FIRINOX
0.5188
0.2200
0.4763
0.1517
Tumor weight (grams)
Ex vivo and in vivo pancreas tumor
Vehicle
FIRINOX + TPL2i
1cm
volume=907.5mm3
volume=896.8mm3
volume=109.8mm3
volume=115.2mm3
3cm

Figure 8. E188K mutation in *MAP3K8*/TPL2 is a gain-of-function mutation

(A) Lollipop plot adapted from CBioPortal.org (as of August 2019) identifying mutations in TPL2/*MAP3K8.* **(B)** Immunoblots of 293T cells transfected with empty expression vector (EV, control) or vector encoding HA epitope tagged TPL2 WT or TPL2 E188K for 48 hours. **(C)** Relative serum-response element (SRE) activity and NFκB reporter activity in 293T cells transfected as in **(B)**. Data is from two independent experiments and *P* values are from two-way ANOVA followed by Tukey's multiple comparison test. **(D)** Heat map representing relative expression in Log_2 units of proteins evaluated by reverse-phase protein array of 293T cells transfected with empty vector (EV, control) or vector encoding HA-tagged TPL2 WT or TPL2 E188K in duplicate ($n = 2$) for 48 hours. **(E)** Relative abundance (in Log_2 units) of the top 15 up-regulated targets in RPPA shown in **(D).** p-ERK (in bold text) is the top hit and significantly upregulated targets are indicated with *P* values from two-way ANOVA with Tukey's multiple comparison test. All error bars indicate mean ± SEM; ****$P<0.0001$, ***$P<0.0002$, **$P<0.0021$, *$P<0.0332$.

Figure 8

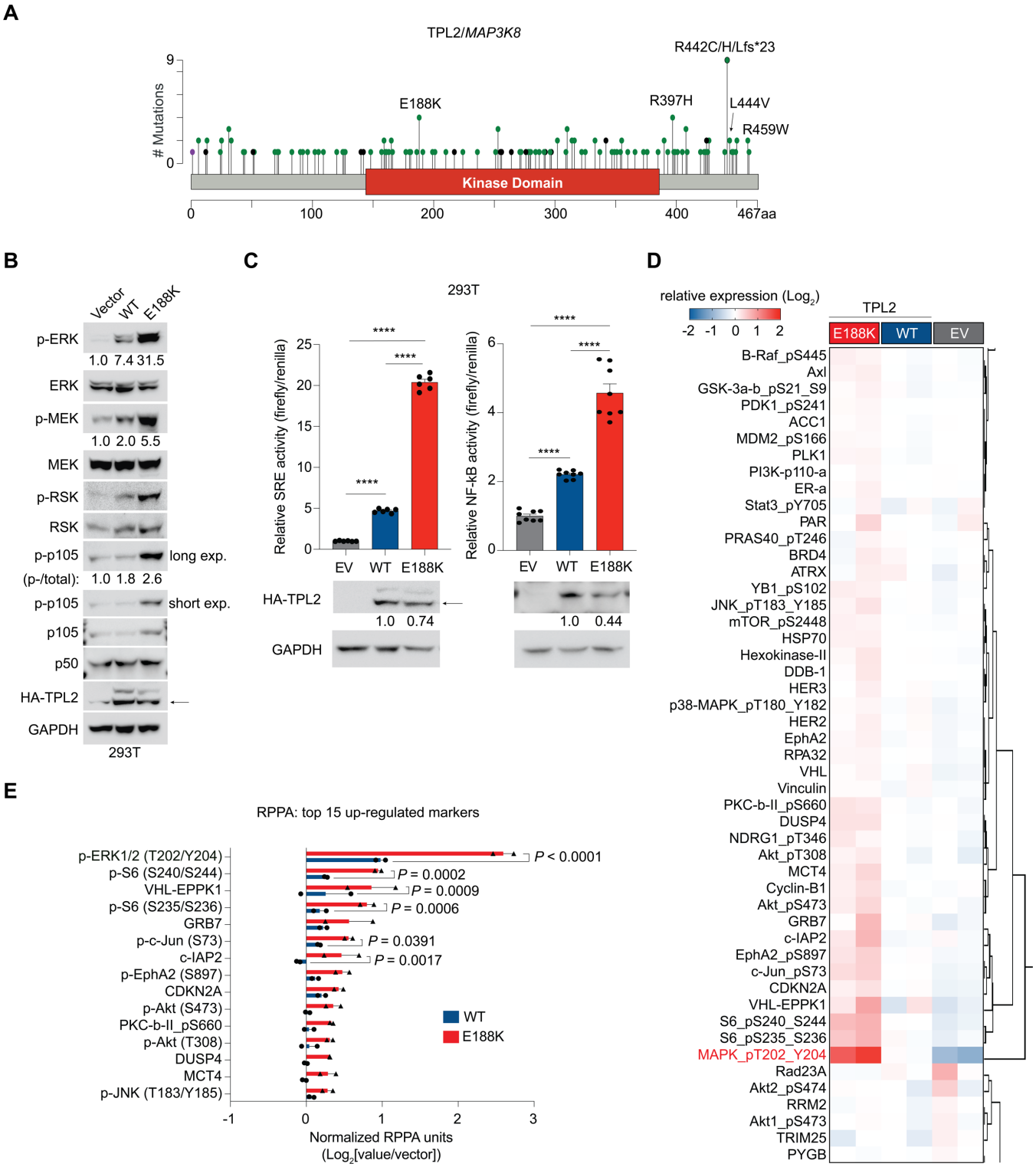

1085

Figure 9. E188K mutation stabilizes TPL2 protein

(A) Immunoblots of HEK T/tH cells stably expressing HA epitope-tagged TPL2 WT or TPL2 E188K treated with 10μg mL^{-1} cycloheximide. Table below shows half-life ($t_{1/2}$) of TPL2 WT and TPL2 E188K protein calculated by measuring HA-TPL2 band intensities, normalizing to t_0 and performing one-phase exponential decay. Data represents one of three independent experiments showing similar results. **(B)** Immuno-precipitation of HA epitope-tagged TPL2 WT or TPL2 E188K treated with 10μM MG132 and immunoblotted as indicated. **(C)** Sanger sequencing peaks of *MAP3K8* (TPL2) locus in Hs695T. Arrow indicates the naturally occurring missense point mutation responsible for Glu→Lys substitution at codon 188 (E188K) in TPL2 in Hs695T cell line. **(D)** Immunoblot of Hs695T cells treated with TPL2i for 24 hours in 10% serum media. **(E)** Proliferation of Hs695T cells treated with TPL2i. *P* values from two-way ANOVA with Dunnett's multiple comparison test. **(F)** Viability of Hs695T cells treated with PLX4032 (BRAFi) alone or in combination with two different concentrations of TPL2i. Graph on right depicts GI_{50} of PLX4032 in Log_{10} units. Data represents 10 replicates from four independent experiments, *P* values are from one-way ANOVA with Dunnett's multiple comparison test. All error bars indicate mean ± SEM; ****P<0.0001, ***P<0.0002, **P<0.0021, *P<0.0332.

Figure 9

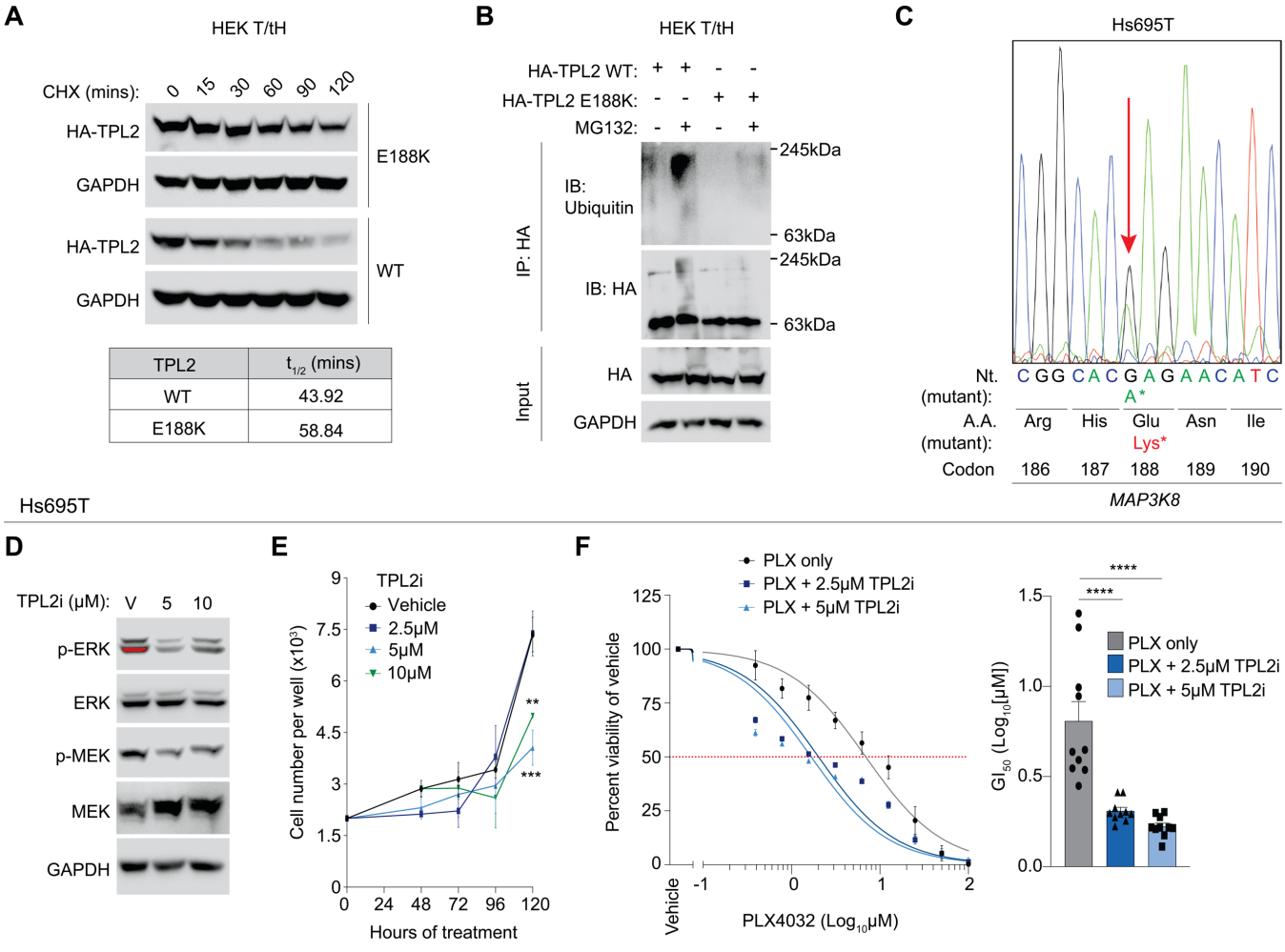
A
HEK T/tH
CHX (mins): 0 15 30 60 90 120
HA-TPL2
GAPDH
E188K
HA-TPL2
GAPDH
WT
TPL2 | t1/2 (mins)
WT | 43.92
E188K | 58.84
B
HEK T/tH
HA-TPL2 WT: + + - -
HA-TPL2 E188K: - - + +
MG132: - + - +
IP: HA
IB: Ubiquitin
245kDa
63kDa
IB: HA
245kDa
63kDa
Input
HA
GAPDH
C
Hs695T
Nt. (mutant): C G G C A C G A G A A C A T C
A*
A.A. (mutant): Arg His Glu Asn Ile
Lys*
Codon 186 187 188 189 190
MAP3K8
Hs695T
D
TPL2i (μM): V 5 10
p-ERK
ERK
p-MEK
MEK
GAPDH
E
TPL2i
Vehicle
2.5μM
5μM
10μM
Cell number per well (x10³)
Hours of treatment
F
PLX only
PLX + 2.5μM TPL2i
PLX + 5μM TPL2i
Percent viability of vehicle
Vehicle
PLX4032 (Log10μM)
GI50 (Log10[μM])
PLX only
PLX + 2.5μM TPL2i
PLX + 5μM TPL2i

Figure 10. R442H is a gain-of-function mutation that curtails proteasomal degradation of TPL2

(A) Immunoblots of 293T cells transiently transfected with empty vector (EV), or vector encoding HA epitope-tagged TPL2 WT or TPL2 R442H for 48 hours. On right is quantification of p-ERK band intensities for TPL2 WT and TPL2 R442H samples from immunoblots on left. Data represents two independent experiments, *P* values from two-way ANOVA with Sidak's multiple comparison test. **(B)** Immunoblots of HEK T/tH cells stably expressing vector encoding TPL2 WT or TPL2 R442H and treated with 10μg mL^{-1} cycloheximide for indicated durations. Table below states half-life ($t_{1/2}$) of TPL2 WT and mutant proteins calculated by measuring HA-TPL2 band intensities, normalizing to t_0 and performing one-phase exponential decay analysis as shown in graph most below. Experiment was performed three times and one set of data is shown. **(C)** Immunoblots of HEK T/tH cells stably expressing empty vector or HA epitope-tagged TPL2 mutants treated with MG132 (10μM) for 4 hours. One of $\geq$2 independent experiments is shown. C-term truncated TPL2 is used as positive control. **(D)** Immunoblots of IGROV1 cells serum starved for 24 hours and treated with TPL2i for 2 hours. **(E)** Immunoblots of IGROV1 cells after shRNA mediated TPL2 depletion. **(F-G)** Proliferation of IGROV1 cells treated with TPL2i and after shRNA mediated TPL2 depletion respectively. *P* values from two-way ANOVA with Dunnett's multiple comparison test. **(H)** 3D organoid growth of IGROV1 cells after shRNA mediated TPL2 depletion and rescue with either WT or R442H mutant. Organoids were counted from four independent transfected wells per condition. Scale bars are 100μm. *P* values from one-way ANOVA with Dunnett's multiple comparison test. All error bars indicate mean ± SEM; ****P<0.0001, ***P<0.0002, **P<0.0021, *P<0.0332.

Figure 10

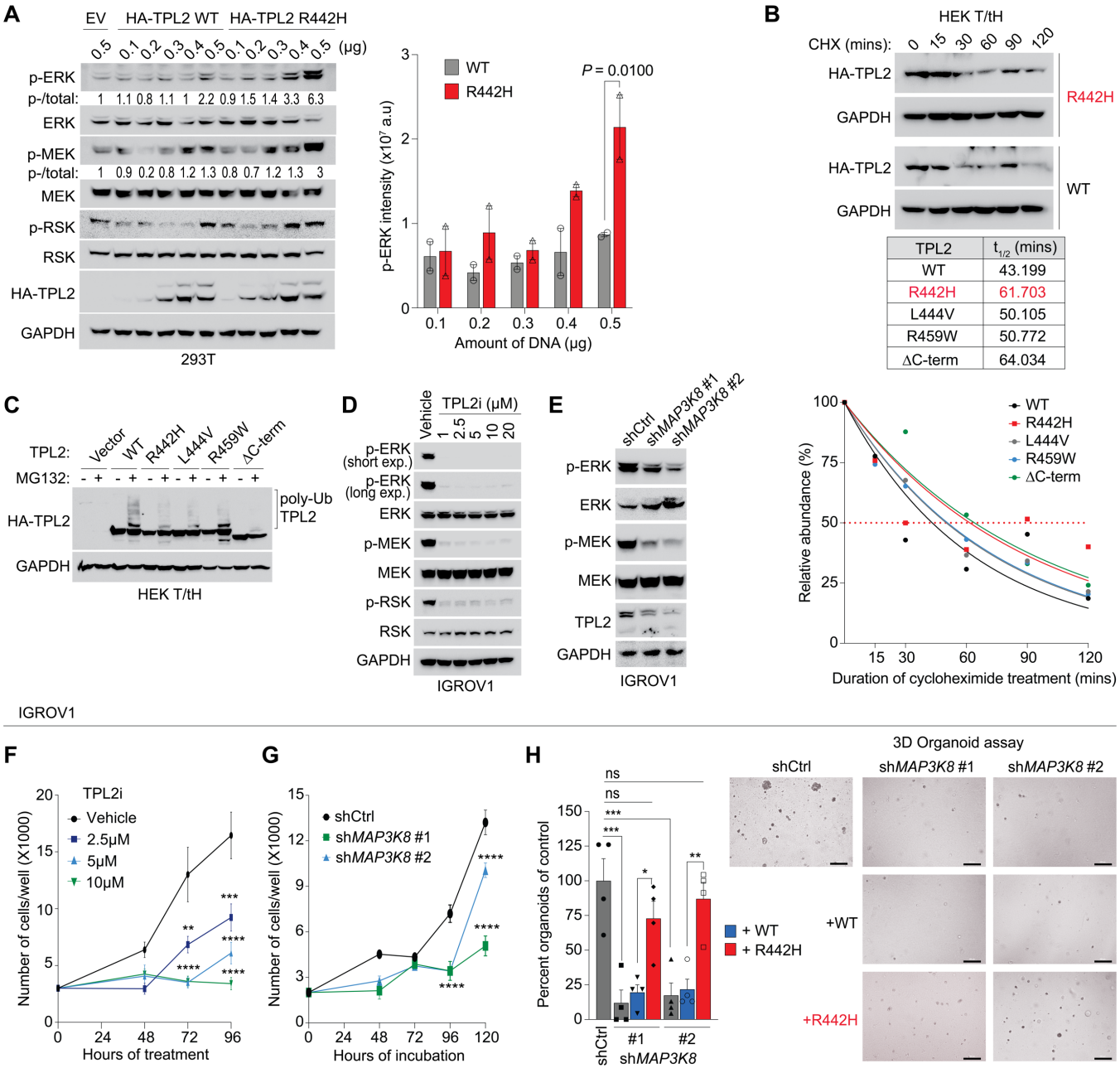
A
EV
HA-TPL2 WT
HA-TPL2 R442H
0.5 0.1 0.2 0.3 0.4 0.5 0.1 0.2 0.3 0.4 0.5 (μg)
p-ERK
p-/total: 1 1.1 0.8 1.1 1 2.2 0.9 1.5 1.4 3.3 6.3
ERK
p-MEK
p-/total: 1 0.9 0.2 0.8 1.2 1.3 0.8 0.7 1.2 1.3 3
MEK
p-RSK
RSK
HA-TPL2
GAPDH
293T
WT
R442H
P = 0.0100
p-ERK intensity (x10^7 a.u)
Amount of DNA (μg)
B
HEK T/tH
CHX (mins): 0 15 30 60 90 120
HA-TPL2
GAPDH
R442H
WT
TPL2 | t1/2 (mins)
WT | 43.199
R442H | 61.703
L444V | 50.105
R459W | 50.772
ΔC-term | 64.034
C
TPL2: Vector WT R442H L444V R459W ΔC-term
MG132: - + - + - + - + - + - +
HA-TPL2
poly-Ub TPL2
GAPDH
HEK T/tH
D
Vehicle
TPL2i (μM) 1 2.5 5 10 20
p-ERK (short exp.)
p-ERK (long exp.)
ERK
p-MEK
MEK
p-RSK
RSK
GAPDH
IGROV1
E
shCtrl
shMAP3K8 #1
shMAP3K8 #2
p-ERK
ERK
p-MEK
MEK
TPL2
GAPDH
IGROV1
WT
R442H
L444V
R459W
ΔC-term
Relative abundance (%)
Duration of cycloheximide treatment (mins)
IGROV1
F
TPL2i
Vehicle
2.5μM
5μM
10μM
Number of cells/well (X1000)
Hours of treatment
G
shCtrl
shMAP3K8 #1
shMAP3K8 #2
Number of cells/well (X1000)
Hours of incubation
H
ns
ns
***
***
*
**
Percent organoids of control
shCtrl
#1
#2
shMAP3K8
+ WT
+ R442H
3D Organoid assay
shCtrl
shMAP3K8 #1
shMAP3K8 #2
+WT
+R442H